Advances in using municipal solid waste incineration (MSWI) bottom ash as precursor for alkali-activated materials

A critical review

Chen, Boyu; Perumal, Priyadharshini; Aghabeyk, Farnaz; Adediran, Adeolu; Illikainen, Mirja; Ye, Guang

DOI
10.1016/j.resconrec.2024.107516

Publication date
2024

Document Version
Final published version

Published in
Resources, Conservation and Recycling

Citation (APA)
Chen, B., Perumal, P., Aghabeyk, F., Adediran, A., Illikainen, M., & Ye, G. (2024). Advances in using municipal solid waste incineration (MSWI) bottom ash as precursor for alkali-activated materials: A critical review. *Resources, Conservation and Recycling*, *204*, Article 107516. https://doi.org/10.1016/j.resconrec.2024.107516

Resources, Conservation & Recycling 204 (2024) 107516

Contents lists available at ScienceDirect

Resources, Conservation & Recycling

journal homepage: www.elsevier.com/locate/resconrec

Review

Advances in using municipal solid waste incineration (MSWI) bottom ash as precursor for alkali-activated materials: A critical review

Boyu Chen [a,*], Priyadharshini Perumal [b], Farnaz Aghabeyk [a], Adeolu Adediran [b], Mirja Illikainen [b], Guang Ye [a,*]

[a] Microlab, Section Materials and Environment, Faculty of Civil Engineering and Geosciences, Delft University of Technology, Stevinweg 1, 2628 CN, Delft, the Netherlands

[b] Faculty of Technology, Fiber and Particle Engineering Research Unit, PO Box 4300, 90014, University of Oulu, Finland

ARTICLE INFO

Keywords:
Municipal solid waste incineration bottom ash
Alkali-activated materials
Reaction
Mechanical properties
Durability
Environmental impacts

ABSTRACT

The pursuit of low-carbon binders as alternatives to Portland cement has sparked interest in developing alkali-activated materials (AAM).[1] Using municipal solid waste incineration (MSWI) bottom ash as precursor for AAM has attracted increasing attention as it offers a sustainable, resource-efficient solution to mitigate the environmental impacts associated with the landfill of MSWI bottom ash. However, the varying properties of MSWI bottom ash present challenges in its wide application as AAM precursor. This review provides a comprehensive overview of advances in MSWI bottom ash-based AAM,[2] with a particular focus on the relationship between the physicochemical properties of MSWI bottom ash and the engineering properties of MSWI bottom ash-based AAM. This work consolidates the most up-to-date understanding of the reaction mechanism and reaction products of MSWI bottom ash, along with the existing knowledge about mix design and microstructure formation of MSWI bottom ash-based AAM. The factors influencing the engineering properties of MSWI bottom ash-based AAM are detailed, and the environmental impacts of MSWI bottom ash-based AAM are reviewed. Ultimately, this review provides recommendations for the standardized and effective use of MSWI bottom ash as AAM precursor.

1. Introduction

According to a report by the World Bank, the amount of municipal solid waste generated across the world is projected to rise from 2.01 billion tons in 2016 to 3.4 billion tons in 2050 (Kaza et al., 2018). This projection considers the expected growth in both the world population and gross domestic product, which are the main factors driving the increase in municipal solid waste generation. As the generation of municipal solid waste grows, the demand for waste incineration is likely to rise accordingly, especially in densely populated areas with limited land availability. The waste-to-energy market is expected to experience a yearly growth rate of 7.4 % (Grand View Research, 2019). The increasing popularity of waste incineration technology equipped with effective air pollution control system stems from its capability to generate energy from waste, reduce the volume of waste sent to landfills, and mitigate environmental pollution caused by waste accumulation in landfills (Kaza et al., 2018; Pan et al., 2015).

In the past few decades, waste-to-energy plants have been increasingly used to process municipal solid waste, with Europe (Eurostat, 2023), the USA (US EPA, 2022), China (NBS, 2022), and India (IRENA, 2022) reporting a rise in the proportion of municipal solid waste treated by incineration. Due to the rapid expansion of waste-to-energy incineration projects, the management of municipal solid waste incineration residue has emerged as a pressing concern at a global scale (Blasenbauer et al., 2020; Chimenos et al., 1999; Eurostat 2023; IRENA, 2022; Kaza et al., 2018; Lin and Lin, 2006; NBS, 2022; Tian et al., 2020; US EPA 2022). The mass of the residue produced after municipal solid waste incineration can reach around 20 % of the waste input (Li et al., 2004;

* Corresponding authors.
E-mail addresses: B.Chen-4@tudelft.nl (B. Chen), G.Ye@tudelft.nl (G. Ye).

[1] Alkali activated materials (AAM) can be categorized into alkali-activated pastes, alkali-activated mortars, and alkali-activated concretes. These three are differentiated by the aggregates. Alkali-activated pastes have no aggregates. Alkali-activated mortars contain only fine aggregates, typically sand. Alkali-activated concretes incorporate both fine aggregates and coarse aggregates (like gravel and crushed stone).

[2] In this text, the term "MSWI bottom ash-based AAM" describes the alkali-activated materials prepared using MSWI bottom ash as a significant component in the precursor.

https://doi.org/10.1016/j.resconrec.2024.107516
Received 29 October 2023; Received in revised form 11 February 2024; Accepted 21 February 2024
Available online 27 February 2024

Phua et al., 2019; Sabbas et al., 2003). Around 80–90 % of municipal solid waste incineration residue is collected at the bottom of the incinerator (Chimenos et al., 1999; Lin and Lin, 2006). This residue is often referred to as municipal solid waste incineration (MSWI) bottom ash. In the United States, about 9 million tons of MSWI ashes were generated in 2017, most of which were MSWI bottom ash (Kumar and Garg, 2022). The European municipal solid waste incineration plants discharge around 20 million tons of bottom ash each year (Šyc et al., 2020). The annual MSWI bottom ash generated in China is more than 13 million tons (Xia et al., 2017).

Currently, MSWI bottom ash is typically landfilled or used after quality-upgrade treatments as a substitute for natural aggregates in road construction and concrete production (Blasenbauer et al., 2020; Dou et al., 2017; Verbinnen et al., 2017; Xuan et al., 2018). Compared with the application as secondary aggregates, using MSWI bottom ash to produce the binders of concrete can help to achieve a higher value application of this industrial by-product. There is a growing interest in using alkali activation technique to transform MSWI bottom ash into a sustainable construction material, which is known as alkali-activated materials (AAM) (Chen et al., 2023a).

AAM is regarded as a sustainable and viable alternative to Portland cement. Portland cement-based concrete is by far the most widely used construction material (Damtoft et al., 2008). The cement industry is responsible for around 8 % of global anthropogenic carbon emissions (Andrew, 2018). Replacing Portland cement with AAM in concrete could reduce 40 to 80 % of its CO_2 emissions (den Heede and De Belie, 2012; Habert, 2013; Habert et al., 2011; Habert and Ouellet-Plamondon, 2016; Heath et al., 2014; McLellan et al., 2011; Ng et al., 2012; Stengel et al., 2009; Weil et al., 2009). Using AAM instead of Portland cement as a building material also helps to reduce the extraction of natural resources. The production of cement is a highly energy- and resource-intensive process that relies heavily on the availability of non-renewable raw materials, such as limestone and fossil fuels (Boesch and Hellweg, 2010). In contrast, AAM is typically synthesized by reacting an aluminosilicate precursor with an alkaline solution. Industrial by-products are usually used as precursors for the production of AAM. The waste-derived activators have the potential to perform similarly to commercial activators (Alnahhal et al., 2021).

The desired properties of AAM for a specific application can be achieved by modifying the mix design, curing condition, and manufacturing process of AAM (Provis, 2018; Provis and Van Deventer, 2013). Compared with Portland cement concrete, well-designed alkali-activated concrete can have comparable or even higher compressive strength, splitting tensile and flexural strength (Xue et al., 2023). The AAM can also outperform Portland cement regarding fire resistance (Xue et al., 2023). In general, the durability of AAM is better than that of Portland cement-based concrete (Wang et al., 2020). The durability performances under consideration include resistance to sulfate attack, acid corrosion, carbonation, and chloride penetration (Wang et al., 2020).

Previous studies have shown that MSWI bottom ash has great potential as a mineral resource to produce AAM (Chen et al., 2023a). Due to the anticipated decline in the supply of conventional AAM precursors, namely blast furnace slag and coal fly ash (IEA, 2009; Provis, 2018; Provis and Van Deventer, 2013), there is a growing need to find alternative industrial by-products. The chemical composition of MSWI bottom ash varies within the same range as coal fly ash (Chen et al., 2023a). Most of the MSWI bottom ash produced in the world contains a significant amount of amorphous phase, more than 50 wt.% (Chen et al., 2023a). The amorphous phase is usually regarded as the major reactive phase in blast furnace slag and Class F coal fly ash (Chancey et al., 2010; Pal et al., 2003). In MSWI bottom ash, the amorphous phase is also the primary reactive phase (Chen et al., 2023b; Tang et al., 2020; Zhu et al., 2019c). Using MSWI bottom ash to produce AAM can be a sustainable solution to the anticipated shortage of coal fly ash (Chen et al., 2023a).

The number of publications using MSWI bottom ash as precursor to prepare AAM has been increasing in recent years. There are several review articles that summarize the current state of knowledge about MSWI bottom ash-based AAM. In 2017, a review paper authored by Silva et al. (Silva et al., 2017) collected case studies about the utilization of MSWI bottom ash to produce AAM. In 2020, Kurda et al. (2020) presented a review to examine the studies on alkali-activated materials prepared using MSWI bottom ash as both single and partial precursors. This review briefly summarized the fresh properties, mechanical properties, and durability of MSWI bottom ash-based AAM. In 2021, Cong and Cheng (2021) published a review paper about the advances in geopolymer materials, in which the feasibility of using MSWI bottom ash as precursor was mentioned. In 2022, Chen et al. (2022) provided an overview of the utilization of municipal solid waste incineration residue as construction materials. In their review article, examples of MSWI bottom ash being used to produce AAM were briefly described. In 2023, Chen et al. (2023a) published a review paper analyzing the compositional diversity and reactivity of MSWI bottom ash sourced from different countries.

Although previous reviews have examined different aspects of MSWI bottom ash-based AAM, a comprehensive analysis is notably absent regarding the mix design, the reaction between MSWI bottom ash and alkaline activator, and the relationship between the physicochemical properties of MSWI bottom ash and the engineering properties of MSWI bottom ash-based AAM. Given the growing interest in using MSWI bottom ash as AAM precursor, the demand for this critical information has become increasingly urgent. Knowledge gained from existing mix design facilitates the development of MSWI bottom ash-based AAM with targeted performance. Understanding the reaction mechanism of MSWI bottom ash provides a theoretical basis for its utilization in AAM production. Establishing the relationship between MSWI bottom ash and the resultant AAM is essential, as it offers insights into the quality-upgrade treatment of MSWI bottom ash. These three aspects constitute the primary focus of this review. Moreover, this work summarizes the compositional characteristics of MSWI bottom ash and discusses quality-upgrade treatments. It offers a comprehensive overview of the leaching potential, durability, and environmental impacts of AAM derived from MSWI bottom ash. The information and insights presented in this review can serve as a valuable reference for future research and ultimately promote the sustainable use of MSWI bottom ash as AAM precursor. Fig. 1 provides a visual overview of the main content covered in this review paper.

2. Chemical properties and quality upgrade treatments of MSWI bottom ash

2.1. Compositional characteristics

2.1.1. Chemical composition

The chemical composition of MSWI bottom ash can vary significantly depending on its source. Fig. 2 illustrates the compositional variation of MSWI bottom ash used for the preparation of AAM. This data was measured by X-ray fluorescence spectrometry (XRF) and was collected for ashes produced in China, Italy, Portugal, Singapore, Spain, Thailand, the UK, and the Netherland. More details of these data can be found in Appendix Table 1. Currently, there is no standardized classification system to organize the diverse compositions of MSWI bottom ash for practical applications. Given that the chemical composition of MSWI bottom ash falls within the same range as that of coal fly ash (Chen et al., 2023b, 2023a), drawing upon the experience gained from coal fly ash could be beneficial (Manz, 1999). Such classification may involve grouping MSWI bottom ash into calcareous (CaO-enriched) and silicious (SiO_2-enriched) types.

2.1.1.1. Major components. As observed in Fig. 2, the major components in MSWI bottom ash are SiO_2, CaO, Al_2O_3, and Fe_2O_3. The SiO_2

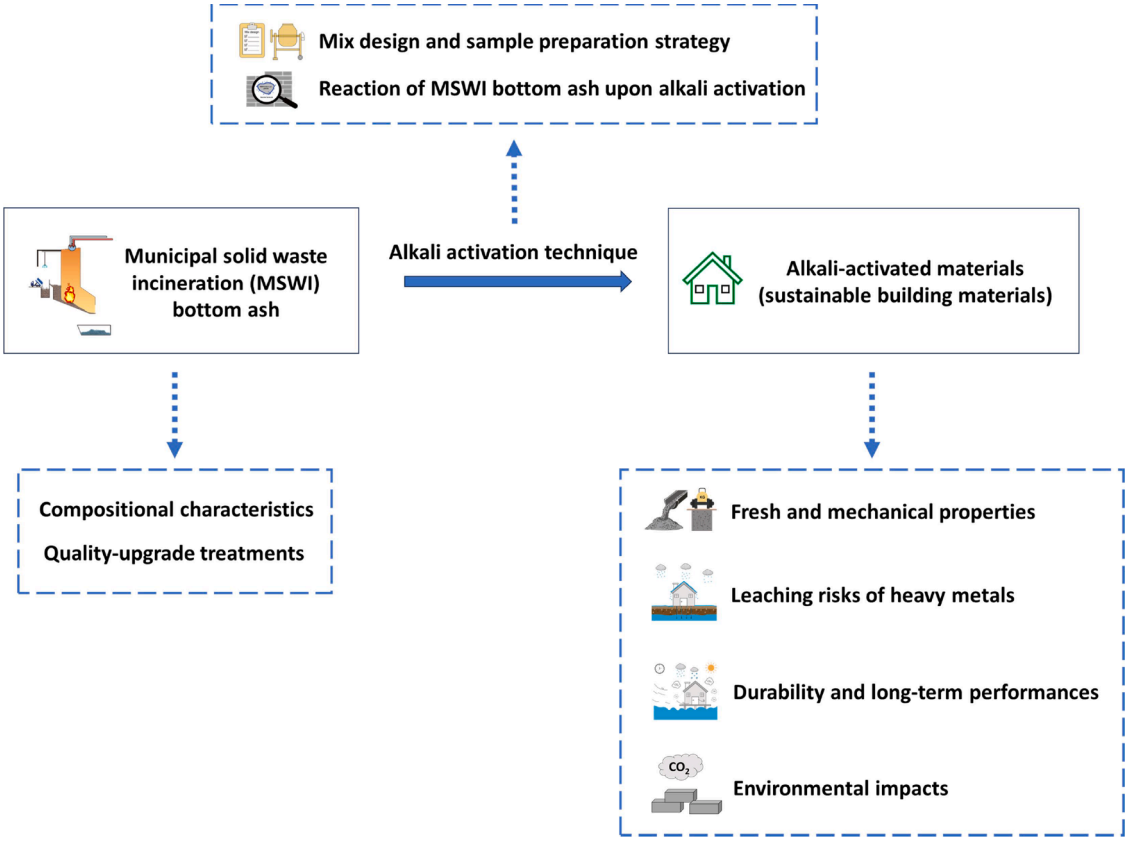

Fig. 1. The outline of this review paper.

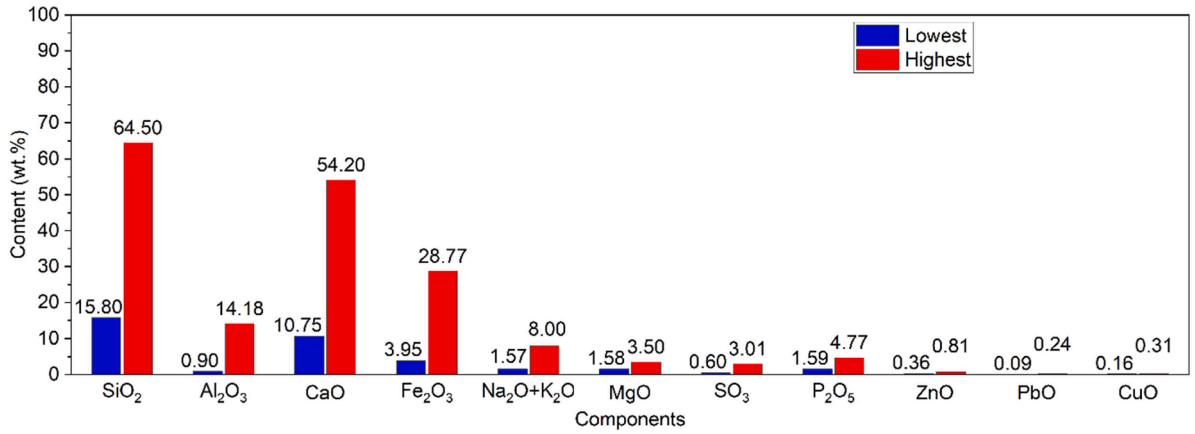

Fig. 2. Ranges of components in MSWI bottom ash, summarized from XRF data in Appendix Table 1.

content varies within a wide range, from 15.8 wt.% to 64.5 wt.%. The amount of CaO detected in MSWI bottom ash also exhibits notable variations, spanning from 10.75 wt.% to 54.2 wt.%. In contrast, the distribution of Al_2O_3 (0.9 - 14.18 wt.%) and Fe_2O_3 (3.95 - 28.77 wt.%) is relatively narrow. Notably, SiO_2 is the most abundant component in MSWI bottom ash across the listed regions (see Appendix Table 1). An exception is found in Thailand, where the CaO content in MSWI bottom ash is higher than the SiO_2 content. Furthermore, Thailand is the only country that produces MSWI bottom ash with a high percentage of K_2O (7.30 wt.%).

2.1.1.2. Heavy metal components. As indicated in Appendix Table 1, some studies focus only on reporting the major components of MSWI bottom ash and do not provide detailed information on heavy metal content. Despite this, it is important to note that the incorporation of heavy metals is one of the major issues that hinder the application of MSWI bottom ash in construction materials due to the potential environmental and health risks from excessive heavy metal leaching (Chen et al., 2023a; Dou et al., 2017). The heavy metals in MSWI bottom ash mainly concentrate in fine fractions (Chen et al., 2023a). Alam et al. (2019) studied the distribution of potentially toxic elements (PTEs) in the MSWI bottom ash fine particles ($\leq$ 125 μm) and found that the most abundant PTEs were zinc (Zn), copper (Cu), lead (Pb), manganese (Mn), and chromium (Cr).

The heavy metals found in MSWI bottom ash are mainly present within its amorphous phases formed after the incineration of municipal solid waste and within its crystalline phases (including calcite, ettringite, hydrous Al-oxides, and hydrous Fe-oxides) generated due to the weathering of fresh MSWI bottom ash (Alam et al., 2019; Chen et al., 2023a). The heavy metals bound to organic substances in MSWI bottom ash also contribute to the release of heavy metals when MSWI bottom ash is in contact with water (Chen et al., 2023a). The loss on ignition (LOI) provides information about the content of organic substances in MSWI bottom ash. The LOI value of MSWI bottom ash varies from a negligible amount in Singapore to 23 wt.% in Thailand, which demonstrates a huge difference in the total organic carbon based on the origin (see Appendix Table 1).

2.1.2. Mineralogical composition

The mineralogical composition of MSWI bottom ash previously used to prepare AAM is summarized in Appendix Table 2. This data was measured by X-ray diffraction (XRD) analysis and was collected for ashes produced in China, Italy, Portugal, Singapore, Spain, Thailand, the UK, and the Netherland. The minerals in MSWI bottom ash were categorized following the classification proposed by Chen et al. (2023a).

2.1.2.1. Crystalline phase. As shown in Appendix Table 2, the presence of minerals belonging to the groups of silicon dioxide, carbonates, silicates, and iron oxides is frequently reported in the literature. Quartz and calcite are identified in all MSWI bottom ash samples, regardless of their origin. Magnetite is the third most commonly detected phase in MSWI bottom ash. Other phases identified by previous researchers include phosphates (calcium-sodium-magnesium phosphate, hydroxyapatite), sulfate (anhydrite), hydroxide (hydrocalumite), metallic aluminum (Al), and so on. It should be noted that numerous studies have documented the detection of metallic Al in MSWI bottom ash used as AAM precursor, as detailed in Appendix Tables 3 and 4. Rather than using XRD, the presence of metallic Al in MSWI bottom ash was detected in a chemical way, especially through the water displacement method (Chen et al., 2024, 2023a).

2.1.2.2. Amorphous phase. The amorphous phase of MSWI bottom ash can serve as a potential source of reactive Si, Al, and Ca species in the alkali-activated reaction (Chen et al., 2023b; Tang et al., 2020; Zhu et al., 2019c). Yet, there is limited information regarding the chemical composition of the amorphous phase in MSWI bottom ash. The proportions of the major components in amorphous phase can be calculated by subtracting their percentages in the crystalline phases from the overall composition of MSWI bottom ash determined by XRF (Chen et al., 2023b). The findings from Chen et al. (2023b) suggest that soda-lime glass is an important source of the amorphous phase in MSWI bottom ash. Nevertheless, the chemical composition of the amorphous phase is not necessarily the same as that of soda-lime glass. The percentages of SiO_2, CaO, Al_2O_3, Fe_2O_3, Na_2O, and MgO present in the amorphous phase of MSWI bottom ash are 34.2 wt.%, 8.8 wt.%, 7.9 wt.%, 6.2 wt.%, 3.8 wt.%, and 1.7 wt.%, respectively. Chen et al. (2023b) also found a compositional similarity between the amorphous phase of MSWI bottom ash and Class F coal fly ash. As illustrated in Fig. 3(a), the data point representing the relative proportions of SiO_2, CaO, and Al_2O_3 in the amorphous phase of MSWI bottom ash falls within the same region as that of the amorphous phase in Class F coal fly ash.

Evaluating the CaO/SiO_2 and SiO_2/Al_2O_3 ratios in the amorphous phase facilitates the identification of MSWI bottom ash with potential high reactivity as AAM precursor (Chen et al., 2023b). The chemical composition data of the amorphous phase can be used as an input to the thermodynamic model to predict the reaction products in alkali-activated MSWI bottom ash[3] (Chen et al., 2023b). The phase

[3] In this text, the term "alkali-activated MSWI bottom ash" refers to the alkali-activated materials prepared only using MSWI bottom ash as the precursor.

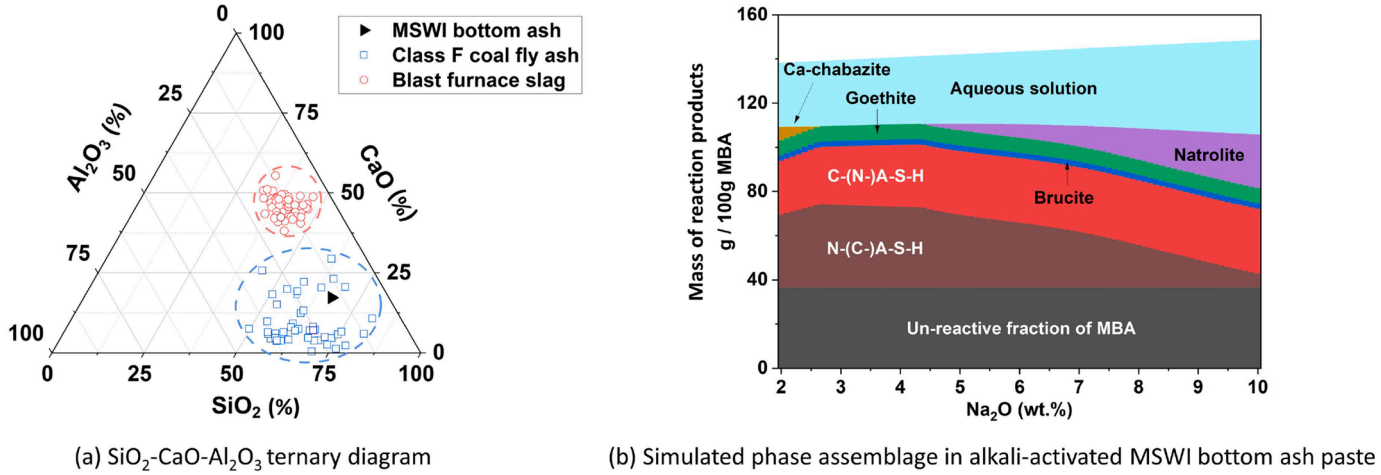

(a) SiO_2-CaO-Al_2O_3 ternary diagram (b) Simulated phase assemblage in alkali-activated MSWI bottom ash paste

Fig. 3. (a) Ternary diagram showing the relative content of SiO_2, CaO, and Al_2O_3. The ternary diagram is plotted according to the weight percentages of the oxides in the amorphous phase of MSWI bottom ash, blast furnace slag, and Class F coal fly ash. (b) Thermodynamically simulated phase assemblage, solid reaction product mass, and pore solution mass after activating 100 g MSWI bottom ash with NaOH solution. The water-to-precursor ratio was kept at 0.35 in the mixture. The simulation was performed with GEMS-Selektor v.3 (Kulik et al., 2013; Wagner et al., 2012). The data is presented as a function of the Na_2O content in the activator. The percentage of Na_2O is with respect to the mass of the precursor. All images are adapted and reprinted from Chen et al. (Chen et al., 2023b) with permission from Elsevier.

assemblages predicted for alkali-activated MSWI bottom ash, as shown in Fig. 3(b), are found to be in good agreement with the experimental findings reported in the literature. The simulation result can serve as a useful reference for the mix design of MSWI bottom ash-based AAM (Chen et al., 2023b).

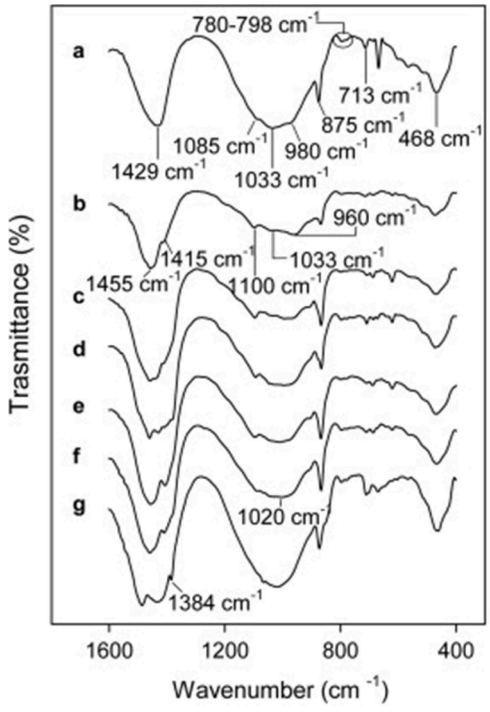

Fig. 4. An example of FTIR spectra showing the chemical bond transformation upon alkali activation of MSWI bottom ash. The spectra illustrate changes over various curing periods: (a) unreacted bottom ash, (b) 1 day, (c) 4 days, (d) 5 days, (e) 7 days, (f) 30 days, and (g) 20 months. This sample was prepared using an activator consisting of 50 wt.% NaOH solution (8 M) and 50 wt.% Na_2SiO_3 solution (SiO_2/Na_2O molar ratio = 3). The sample was cured at room temperature. Reprint from (Lancellotti et al., 2015) with permission from Elsevier.

2.2. Quality upgrade treatments

The quality of MSWI bottom ash needs to be improved before it can be used for AAM production. Detailed specifications of the quality-upgrade treatments from previous research are provided in Appendix Tables 3 and 4. Various methods have been proposed to solve the issues of MSWI bottom ash, such as high metallic Al content, low reactivity, heterogeneous composition, large particle size, and excessive leaching of heavy metals. MSWI bottom ash is usually mixed with alkaline solution to lower its metallic Al content (Casanova et al., 2021; Huang et al., 2019b). While the reactivity of MSWI bottom ash is similar to that of Class F coal fly ash in some cases (Chen et al., 2023b; Joseph et al., 2019), MSWI bottom ash is generally characterized by lower reactivity, especially when compared with blast furnace slag (Chen et al., 2023a, 2023b). The reactivity of MSWI bottom ash can be enhanced by reducing its particle size (Wongsa et al., 2017) or modifying its mineralogical composition (Qiao et al., 2008a, 2008b; Tang et al., 2016). The particle size of MSWI bottom ash is usually reduced by milling, which also helps to improve the homogeneity of the composition of MSWI bottom ash. After milling, the metallic Al can be separated from ground MSWI bottom ash by sieving (Casanova et al., 2021; Chen et al., 2024, 2016; Maldonado-Alameda et al., 2020a; 2020b, 2023, 2021b; Zhang et al., 2023; Zhu et al., 2018a). The risk of excessive heavy metal leaching is usually mitigated by the weathering process to stabilize the heavy metal in MSWI bottom ash (Chen et al., 2023a). It is worth noting that a systematic guideline for selecting these techniques is currently lacking. Most of the proposed pre-treatment methods are only found to be effective at the lab scale.

3. Reaction between MSWI bottom ash and alkaline activator

As presented in Appendix Table 3, the activators, including NaOH solution, water glass solution, hydrated lime, and a mixture of water glass solution and NaOH solution, were used by previous researchers to prepare alkali-activated MSWI bottom ash. Among all these activators, a mixture of water glass solution and NaOH solution is the most commonly used. Although there is a wide variety in the concentration of NaOH solution and the types of water glass solution, the mass ratio between water glass solution and NaOH solution is usually set to be above one. This section focuses on the reaction process and reaction products of MSWI bottom ash when the mixture of water glass solution

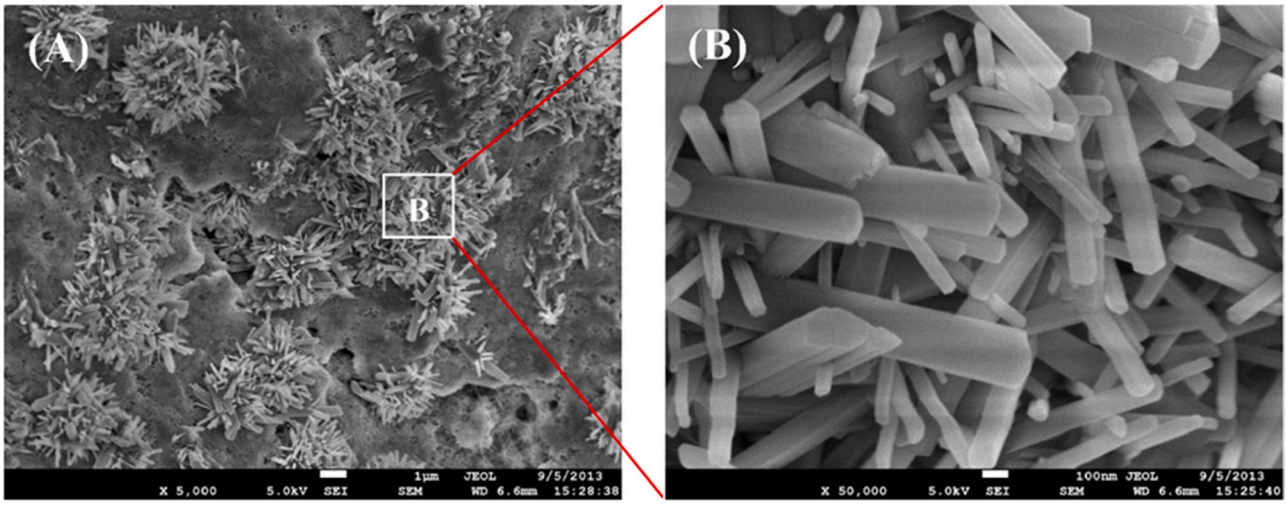

Fig. 5. Scanning Electron Microscopy (SEM) showcasing the fracture surface of 3-day alkali-activated MSWI bottom ash paste: (a) Overview of the fracture surface at the magnification of 5000, (b) enlarged area within image (a) displaying details at a magnification of 50,000. This sample was prepared using an activator consisting of NaOH solution and Na_2SiO_3 solution in a mass ratio of 1:2. The sample was cured at 75°C for 3 days. Adapted and reprinted from (Chen et al., 2016) with the permission from Elsevier.

and NaOH solution is used as activator to prepare AAM.

3.1. Characteristic chemical bond transformation in MSWI bottom ash upon alkali activation

The reaction between MSWI bottom ash and alkaline activator can be monitored by detecting the position and shape change of the broadband centered at the wavenumber between 1200 and 900 cm^{-1} with Fourier Transform Infrared Spectroscopy (FTIR). This broadband, which is found in the spectra of both unreacted MSWI bottom ash and alkali-activated MSWI bottom ash, can be assigned to the stretching vibrations of Si–O (Yu et al., 1999). The Si-O band detected in alkali-activated MSWI bottom ash is narrower and located at a lower wavenumber than that found in the spectrum of unreacted MSWI bottom ash (Chen et al., 2016; Giro-Paloma et al., 2017; Maldonado-Alameda et al., 2020a, 2021a). The higher the alkalinity of the activator, the more the Si-O band will shift to the lower wavenumber upon the activation of MSWI bottom ash (Maldonado-Alameda et al., 2020a, 2021a). This band shifting can be attributed to the inclusion of aluminum in the calcium silicate hydrate (C-S-H) gel (Walkley et al., 2016) and the formation of N-A-S-H gel (Fernández-Jiménez and Palomo, 2005).

For example, Lancellotti et al. (2015) studied the chemical bond transformation when MSWI bottom ash was reacting with the activator made from 50 wt.% NaOH solution (8 M) and 50 wt.% Na_2SiO_3 solution (SiO_2/Na_2O molar ratio = 3). The alkali-activated paste samples were cured at room temperature. According to their FTIR analysis (see Fig. 4), the polymerization is believed to have started within the first 3 h of curing, since a shifting of the Si-O-M (M = Si or Al) band, from 980 cm^{-1} to 940 cm^{-1}, was observed (Lancellotti et al., 2015; Prud'homme et al., 2013). As illustrated in Fig. 4, after 1 day of curing, two shoulder bands appeared at the wavenumber of 1100 and 960 cm^{-1}, which are attributed to the internal vibrations of dissolved $[SiO_4]^{4-}$ and $[AlO_4]^{5-}$ tetrahedra, respectively. The appearance of these two shoulder bands is accompanied by the intensity decrease of the broadband (Si-O-Si band) centered at 1033 cm^{-1} of unreacted MSWI bottom ash. Between 4 and 30 days, the band at 1033 cm^{-1} disappeared, and a new band attributed to the asymmetric stretching of Si-O-Al became visible at 960 cm^{-1} (Mozgawa and Deja, 2009; Rees et al., 2007). After 30 days, the band at 960 cm^{-1} shifted to 1020 cm^{-1}, suggesting that a new aluminosilicate network was formed (Lancellotti et al., 2015).

3.2. Reaction products of MSWI bottom ash

The dissolution of MSWI bottom ash provided Si and Al monomers for the aluminosilicate gel formation (Lancellotti et al., 2015). Rod-like reaction products were observed on the fracture surface of alkali-activated MSWI bottom ash, which was prepared using an activator consisting of a NaOH solution and a Na_2SiO_3 solution (see Fig. 5). Table 1 provides a detailed list of the reaction products that can form after the reaction between MSWI bottom ash and alkaline activator. Previous studies have shown that the alkali activation of MSWI bottom ash mainly leads to the formation of amorphous gel phases, including the C-S-H gel, the sodium aluminosilicate hydrate (N-A-S-H) gel, and the calcium aluminosilicate hydrate (C-A-S-H) gel. The type of gel phase formed in alkali-activated MSWI bottom ash is strongly influenced by the relative content of SiO_2, CaO and Al_2O_3 in the reactive phases of MSWI bottom ash. Maldonado-Alameda et al. (2023) reported that the alkali activation of MSWI bottom ash with high SiO_2 and CaO contents but a low Al_2O_3 content favored the formation of C-S-H gel, rather than N-A-S-H gel or C-A-S-H gel. In addition to the amorphous reaction

Table 1
Reaction products derived from alkali activation of MSWI bottom ash.

Reaction products		References
Amorphous phases	Calcium silicate hydrate (C-S-H) gel	(Huang et al., 2020a; Maldonado-Alameda et al., 2020a; Zhu et al., 2018a)
	Sodium aluminosilicate hydrate (N-A-S-H) gel	(Zhu et al., 2019a)
	Calcium aluminosilicate hydrate (C-A-S-H) gel	(Maldonado-Alameda et al., 2020a)
Crystalline phases	Tobermorite ($Ca_5(Si_6O_{16})(OH)_2$)	(Huang et al., 2020a)
	Hillebrandite ($Ca_2(SiO_3)(OH)_2$)	(Huang et al., 2020a)
	Pirssonite ($Na_2Ca(CO_3)_2{\cdot}2H_2O$)	(Zhu et al., 2018a)
	Gehlenite ($Ca_2Al(AlSi)O_7$) Albite ($NaAlSi_3O_8$)	(Huang et al., 2020a; Maldonado-Alameda et al., 2021a)
	Gismondine ($CaAl_2Si_2O_8{\cdot}4H_2O$)	(Maldonado-Alameda et al., 2020a)

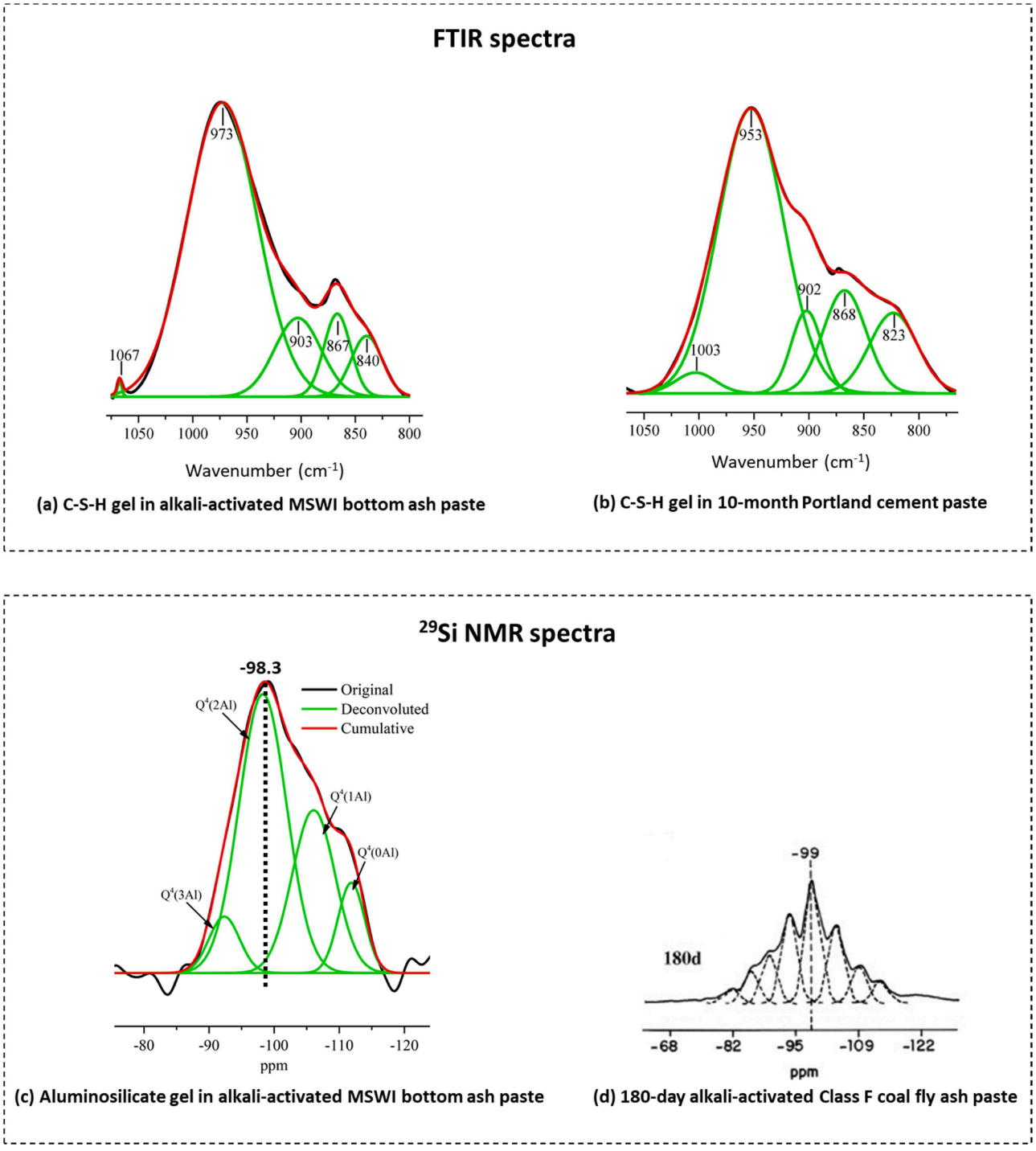

Fig. 6. (a) FTIR spectrum of C-S-H gel extracted from alkali-activated MSWI bottom ash paste (black curve is the original spectrum, green curves are bands due to individual components, and the red curve is the sum of the individual components). This paste was prepared by mixing MSWI bottom ash and activator consisting of NaOH solution (8 M) and Na_2SiO_3 solution. The AAM sample was cured at 75 °C for 3 days (Zhu et al., 2018a). (b) FTIR spectrum of C-S-H gel extracted from 10-month Portland cement paste (Zhu et al., 2018a). (c) ^{29}Si NMR spectrum of aluminosilicate gel in alkali-activated MSWI bottom ash paste. This paste was prepared by mixing MSWI bottom ash and activator consisting of NaOH solution (8 M) and Na_2SiO_3 solution. The AAM sample was cured at 75 °C for 3 days (Zhu et al., 2019a). (d) ^{29}Si NMR spectrum of 180-day alkali-activated Class F coal fly ash paste. This paste was prepared using 100 % Class F coal fly ash as precursor. The chemical composition of the activator is 7.84 wt.% Na_2O, 5.4 wt.% SiO_2, and 86.76 wt.% water. The paste was cured in an oven at 85 °C for 180 days (Criado et al., 2008). All images are reprinted with the permission of Elsevier.

products, the detection of crystalline reaction products was also reported by previous researchers, such as tobermorite ($Ca_5(Si_6O_{16})(OH)_2$), hillebrandite ($Ca_2(SiO_3)(OH)_2$), pirssonite ($Na_2Ca(CO_3)_2{\cdot}2H_2O$), gehlenite ($Ca_2Al(AlSi)O_7$), albite ($NaAlSi_3O_8$), and gismondine ($CaAl_2Si_2O_8{\cdot}4H_2O$).

The C-S-H gel and N-A-S-H gel formed in alkali-activated MSWI bottom ash were found to be similar to the C-S-H gel generated after cement hydration and the N-A-S-H gel formed in alkali-activated Class F coal fly ash, respectively. Zhu et al. (2019a, 2018a) selected the mixture of NaOH solution and Na_2SiO_3 solution as activator to react with fresh MSWI bottom ash. The alkali-activated MSWI bottom ash paste samples were cured at 75 °C for 3 days. The MSWI bottom ash was collected from Singapore. According to the FTIR analysis (see Fig. 6(a) and (b)), the chemical structure of the C-S-H gel found in alkali-activated MSWI bottom ash paste was analogous to that of the C-S-H identified in 10-month Portland cement paste (Zhu et al., 2018a). The main difference was that the C-S-H gel identified in alkali-activated MSWI bottom ash paste had a higher degree of polymerization of the silicate chains (Zhu et al., 2018a). In the ^{29}Si Nuclear Magnetic Resonance (NMR) Spectroscopy spectrum of the N-A-S-H gel extracted from alkali-activated MSWI bottom ash paste (see Fig. 6(c)), the main peak was observed at around −99 mm, corresponding to Al-substituted Si units of $Q^4(2Al)$. As illustrated in Fig. 6(d), the same ^{29}Si NMR resonance appeared in the measurement of 180-day alkali-activated Class F coal fly ash paste (Criado et al., 2008), indicating that the nanostructure of the N-A-S-H gel formed in alkali-activated MSWI bottom ash paste resembles that detected in alkali-activated Class F coal fly ash paste.

The formation of C-A-S-H gel in alkali-activated MSWI bottom ash can be influenced by the alkalinity of the activator. Maldonado-Alameda et al. (2020a, 2021a) activated weathered MSWI bottom ash using a mixture of water glass solution and NaOH solution. The mass ratio between water glass solution and NaOH solution was fixed at four, while the concentration of NaOH solution was varied from 2 M to 8 M. The salicylic acid/methanol (SAM) extraction analysis was used to quantify the amount of C-A-S-H gel formed in alkali-activated MSWI bottom ash paste (García Lodeiro et al., 2009). It was found that when the NaOH concentration increased from 2 M to 6 M, the amount of C-A-S-H gel detected in alkali-activated MSWI bottom ash paste also increased. However, further increasing the NaOH molarity to 8 M did not increase the content of C-A-S-H gel (Maldonado-Alameda et al., 2020a).

The gel formed in alkali-activated MSWI bottom ash is different from the gel obtained after the alkali activation of the glass fraction of MSWI bottom ash, although the amorphous phase present in MSWI bottom ash mainly consists of waste glass particles (Zhu et al., 2019b). The chemical composition of these waste glass particles is almost the same as soda-lime silicate glass (Sinton and LaCourse, 2001; Zhu et al., 2019b). Zhu et al. (2019b) activated the glass fraction separated from fresh MSWI bottom ash with the activator consisting of Na_2SiO_3 solution and 14 M NaOH solution. The main reaction product detected in synthesized alkali-activated paste was the sodium silicate gel (Zhu et al., 2019b). This gel is unstable under a moisture environment and may result in strength loss (Redden and Neithalath, 2014). It is recommended to improve the hydrolytic stability of sodium silicate gel by providing supplementary Ca and Al to promote the formation of C-A-S-H and N-A-S-H gels (Zhu et al., 2019c).

4. AAM prepared with MSWI bottom ash as precursor

4.1. Fresh properties of alkali-activated MSWI bottom ash

Previous studies on the fresh properties of alkali-activated MSWI bottom ash examined water-to-binder ratio, workability, consistency, density of fresh mixture, and setting. Casanova et al. (2021) found that the water requirement of alkali-activated MSWI bottom ash mortar was high. In this case, the lignosulphonate-based water reducer, commonly used to improve the workability of Portland cement paste, was employed to control the water-to-binder ratio and modify the workability of alkali-activated MSWI bottom ash mortar (Carvalho et al., 2021; Casanova et al., 2021). However, the extent to which this water reducer can enhance workability was not mentioned. It is important to note that the effectiveness of plasticizer is strongly influenced by the composition of the precursor and the type of activator AAM (Liu et al., 2023). Most conventional plasticizers used in Portland cement are found to be ineffective in adjusting the workability of AAM. It is recommended to formulate a water reducer in according to the characteristics of AAM (Liu et al., 2023).

The slump value of alkali-activated MSWI bottom ash mortar was much lower than that of Portland cement mortar and alkali-activated Class F coal fly ash mortar (Carvalho et al., 2021). This low slump value was thought to be related to the irregular, angular, and flattened shape of MSWI bottom ash particles (Carvalho et al., 2021). The density of fresh alkali-activated MSWI bottom ash mortar was lower than that of fresh alkali-activated Class F coal fly ash mortar and Portland cement mortar because MSWI bottom ash used by Carvalho et al. (2021) contained metallic Al.

In terms of setting, the fresh mixture of alkali-activated MSWI bottom ash cured at room temperature requires more than 24 h to set (Casanova et al., 2021; Chen et al., 2023b; Qiao et al., 2008c, 2008b). Chen et al. (2023b) found that the reactivity of MSWI bottom ash as AAM precursor was similar to that of Class F coal fly ash, but much lower than that of blast furnace slag. The slow setting of alkali-activated MSWI bottom ash can be explained by the dissolution behavior of MSWI bottom ash under alkaline condition (Chen et al., 2023b). When mixing MSWI bottom ash with NaOH solution (4 M, 5 M, or 6 M), the molar ratio of Si and Al released by MSWI bottom ash at room temperature was far below the optimal value proposed by Duxson et al. (2005). This low

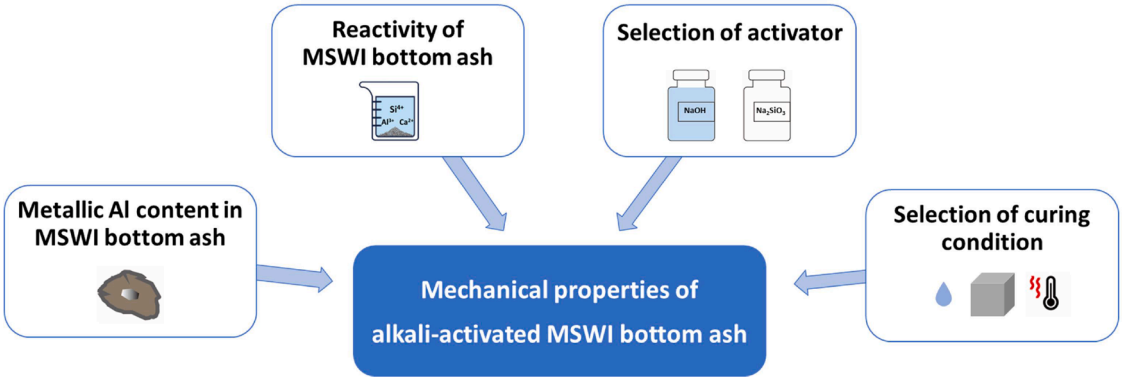

Fig. 7. Factors influencing the mechanical properties of alkali-activated MSWI bottom ash.

Si/Al molar ratio is not favorable for the early-age strength development of alkali-activated MSWI bottom ash (Chen et al., 2023b). To solve the issue of slow setting, increasing the Si/Al ratio in the mixture of precursor and activator is a recommended approach, which can be achieved by adding Si-enriched precursors or Na_2SiO_3 solution (Chen et al., 2023b).

Other possible solutions to the slow setting issue are the thermal curing of fresh mixture and the reactivity improvement of MSWI bottom ash. Casanova et al. (2021) prepared alkali-activated MSWI bottom ash mortar with 10 M NaOH solution. The fresh mortar mixture did not set after one week under ambient conditions. To accelerate the reaction of MSWI bottom ash, Casanova et al. (2021) cured the fresh mortar mixture at 70 or 90 °C. Qiao et al. (2008c, 2008b) activated MSWI bottom ash with hydrated lime and found that the paste prepared with 100 % MSWI bottom ash had a final setting time of 52 h. The problem of slow setting was solved by performing thermal treatments on MSWI bottom ash to promote the formation of reactive crystalline phases. Alkali-activated MSWI pastes prepared with 700 °C treated MSWI bottom ash achieved final set after 9 min (Qiao et al., 2008b).

4.2. Mechanical properties of alkali-activated MSWI bottom ash

The mechanical properties of alkali-activated MSWI bottom ash are mainly influenced by four factors: metallic Al content in MSWI bottom ash, reactivity of MSWI bottom ash, selection of activator, and selection of curing condition (see Fig. 7).

4.2.1. Influence of the metallic Al content in MSWI bottom ash

As illustrated in Appendix Table 3, most of the MSWI bottom ash used for AAM preparation contains metallic Al. The metallic Al embedded in MSWI bottom ash particles usually works as the foaming agent, resulting in volume expansion and low compressive strength of alkali-activated MSWI bottom ash (Carvalho et al., 2021; Casanova et al., 2021; Huang et al., 2020a; Lancellotti et al., 2015; Maldonado-Alameda et al., 2020a). The volume expansion caused by the release of hydrogen gas is restrained by alkali-activated MSWI bottom ash paste, which would crack once the internal stress induced by volume expansion exceeds its strength (Chen et al., 2020). Huang et al. (2020a) prepared alkali-activated mortars with MSWI bottom ash containing 1.92 wt.% metallic Al. After curing for three days at room temperature, the alkali-activated MSWI bottom ash mortars showed no strength, and severe defects, such as voids and interconnecting pores, were observed on the specimens. The 28-day compressive strength only reached 2.4 MPa.

In addition to the quality-upgrade treatment of MSWI bottom ash, the following methods were also used by previous researchers to minimize the negative effects of metallic Al on the compressive strength of alkali-activated MSWI bottom ash:

- Method one is to prolong the mixing time of fresh pastes or cast freshly mixed pastes a few tens of minutes later during the preparation of alkali-activated MSWI bottom ash. The extension of mixing time accelerates the oxidation of metallic Al and facilitates the escape of hydrogen gas from fresh alkali-activated pastes (Chen et al., 2016). A delay in the casting of fresh alkali-activated pastes provides sufficient time for the corrosion of metallic Al under alkaline conditions, making it possible to remove all the hydrogen gas released from the redox reaction of metallic Al via the vibration of fresh pastes (Carvalho et al., 2021; Casanova et al., 2021). Once entrained hydrogen gas is emitted from fresh pastes, the volume expansion of AAM can be dramatically reduced. It is worth noting that the feasibility of this method depends on the setting time of alkali-activated MSWI bottom ash.
- Method two is to reduce the amount of water used for the preparation of alkali-activated MSWI bottom ash. When MSWI bottom ash contains metallic Al, alkali-activated MSWI bottom ash prepared at a lower water-to-solid ratio exhibits higher compressive strength (Chen et al., 2016; Qiao et al., 2008c). The adverse effect of metallic Al content on the compressive strength of alkali-activated MSWI bottom ash is smaller at a lower water-to-solid ratio. Qiao et al. (2008c) compared the alkali-activated MSWI bottom ash paste prepared at two different water-to-solid ratios: 0.2 and 0.5. The voids caused by hydrogen gas release were only observed in alkali-activated MSWI bottom ash paste prepared with the water-to-solid ratio of 0.5.
- Method three is to separate MSWI bottom ash according to the metallic Al content and only use the fraction that contains the lowest amount of metallic Al to prepare AAM. Zhu et al. (2019c) separated the fresh MSWI bottom ash into non-ferrous, ferrous, and glass fractions. Among these three fractions, the metallic Al content in the glass fraction is the lowest, while the non-ferrous fraction has the highest metallic Al content. The 3-day compressive strength of the alkali-activated paste prepared with 100 % glass fraction reached up to 31.69 MPa.

4.2.2. Influence of the reactivity of MSWI bottom ash

Apart from metallic Al, the low reactivity of MSWI bottom ash is also responsible for the low compressive strength of alkali-activated MSWI bottom ash. Qiao et al. (2008b) used weathered MSWI bottom ash to prepare AAM and found that the 28-day compressive strength of alkali-activated MSWI bottom ash paste was very low. The compressive strength increased significantly after improving the reactivity of MSWI bottom ash via thermal treatment (at 700 °C). The 28-day compressive strength of the alkali-activated paste prepared with thermally treated MSWI bottom ash was around 2.9 MPa, much higher than that of the alkali-activated paste made from untreated MSWI bottom ash (about 0.6 MPa) (Qiao et al., 2008b).

4.2.3. Influence of activator

The alkalinity of the activator is an important factor that influences the compressive strength of alkali-activated MSWI bottom ash. Carvalho et al. (2021) found that MSWI bottom ash dissolved more easily in NaOH solution than in Na_2SiO_3 solution due to the higher alkalinity of NaOH solution. NaOH solution-activated MSWI bottom ash mortar had higher compressive strength than Na_2SiO_3 solution-activated MSWI bottom ash mortar. The compressive strength of NaOH solution-activated MSWI bottom ash mortars increased as the concentration of NaOH solution increased from 4 to 10 mol/kg. Chen et al. (2016) reported that the alkalinity of the activator prepared with Na_2SiO_3 solution and 4 M NaOH solution was too low to activate MSWI bottom ash. When the concentration of NaOH solution increased from 4 M to 8 M, hardened paste samples were obtained as the result of an increased pH of the activator and the release of more monomers from the dissolution of MSWI bottom ash.

When MSWI bottom ash is activated with a mixture of water glass solution and NaOH solution, the alkalinity and the alkali modulus (Ms) of the activator (the molar ratio between SiO_2 and Na_2O) can both influence the compressive strength of alkali-activated MSWI bottom ash. Maldonado-Alameda et al. (2021a) activated weathered MSWI bottom ash using a mixture of water glass solution and NaOH solution. A dramatic increase in compressive strength was observed after increasing the concentration of NaOH solution from 2 M to 6 M. However, further increasing the concentration of NaOH solution to 8 M led to a strength reduction in synthesized alkali-activated MSWI bottom ash paste. Maldonado-Alameda et al. (2021a) found the optimum modulus of the activator to be in the range of 2.0–2.5.

4.2.4. Influence of curing condition

The curing temperature strongly influences the early-age compressive strength of alkali-activated MSWI bottom ash. When alkali-activated MSWI bottom ash was cured at room temperature, the 1-day compressive strength could still be too low for demolding (Maldonado-Alameda et al., 2020a, 2021a; Qiao et al., 2008c, 2008b). In this case,

alkali-activated MSWI bottom ash was demolded after curing at room temperature for three days (see Appendix Table 3). The early-age compressive strength of alkali-activated MSWI bottom ash can be increased by curing at an elevated temperature. In previous research, thermal curing was performed at a temperature between 70 and 90 °C, and the curing period varied from one to three days (Carvalho et al., 2021; Casanova et al., 2021; Chen et al., 2016; Maldonado-Alameda et al., 2023; Zhu et al., 2019b, 2019c).

4.3. Leaching of contaminants from alkali-activated MSWI bottom ash

The leaching of contaminants from alkali-activated MSWI bottom ash into the environment can be higher than that from MSWI bottom ash. Maldonado-Alameda et al. (2020c) found that large quantities of heavy metals were detected in the leachate after dissolving weathered MSWI bottom ash in 8 M NaOH solution. Chen et al. (2016) reported that alkali activation of MSWI bottom ash increased the leaching of Cr. Test results of Giro-Paloma et al. (2017) also indicated that the amount of arsenic (As) leached from alkali-activated MSWI bottom ash paste was 30 to 40 times as much as that detected in the leachate of MSWI bottom ash powder. The antimony (Sb) and Zn in the leachate of alkali-activated MSWI bottom ash paste rose to more than 5 times their concentrations in the leachate of MSWI bottom ash powder (Giro-Paloma et al., 2017). It is worth mentioning that Chen et al. (2016) and Giro-Paloma et al. (2017) did not mention whether the MSWI bottom ash had been weathered or not during plant-scale treatments.

The leaching of heavy metals from alkali-activated MSWI bottom ash could exceed the regulatory limit. Maldonado-Alameda et al. (2020a, 2023, 2021a) used weathered MSWI bottom ash to prepare AAM and found that the leaching of As and Sb from alkali-activated MSWI bottom ash paste exceeded the required limit of non-hazardous waste. The excessive leaching of these two metals can be related to the waste glass present in MSWI bottom ash, as As_2O_3 and Sb_2O_3 are usually used in the glass industry as fining agents to lighten glass and remove air bubbles (Apostoli et al., 1998). When the pH of the activator became higher, more heavy metals would leach out from alkali-activated MSWI bottom ash paste, especially for the elements that were initially present in waste glass particles (Maldonado-Alameda et al., 2020a). Zhu et al. (2019c) also found that alkali activation of the waste glass present in MSWI bottom ash promoted the leaching of Zn, Ni, Pb, and Cr, as compared with the leaching of unreacted waste glass.

4.4. Durability of alkali-activated MSWI bottom ash

Understanding the durability characteristics of alkali-activated materials is crucial for determining the most effective mixtures and ensuring their reliability in various aggressive environments (Bernal and Provis, 2014). Alkali-activated materials can experience significant deterioration in scenarios that include exposure to high concentrations of CO_2, sulfates, chlorides, or acid, severe temperature fluctuations like freeze-thaw cycles, or conditions conducive to alkali-silica reaction or efflorescence (Arbi et al., 2016; Bernal and Provis, 2014; Nodehi et al., 2022; Wang et al., 2020; Wang and Noguchi, 2020). However, research on the durability of alkali-activated MSWI bottom ash is currently very limited.

In previous research, mainly the carbonation resistance of alkali-activated MSWI bottom ash was studied. Carvalho et al. (2021) prepared alkali-activated MSWI bottom ash mortars with NaOH solution and Na_2SiO_3 solution, respectively. The results indicated that the carbonation of all mortar samples was completed after 28 days inside the carbonation chamber (at 23 ± 3 °C, 60 ± 5 % relative humidity, and a CO_2 concentration of 5 ± 0.1 %). This fast carbonation is mainly attributed to the porous structure of alkali-activated MSWI bottom ash mortars, which facilitates the diffusion of CO_2. It is important to note that the carbonation of alkali-activated materials is also a chemically controlled process. The chemistry of the pore solution, particularly the pH, and the carbonation resistance of the reaction products formed after the alkali activation reaction, such as the C-A-S-H and N-A-S-H gels, significantly influence the carbonation resistance of alkali-activated materials (Bernal et al., 2013, 2012). However, these two influencing factors have not been thoroughly studied in the case of alkali-activated MSWI bottom ash.

Although alkali-activated MSWI bottom ash mortar samples exhibited poor carbonation resistance, a dramatic strength improvement was observed after they were exposed to accelerated carbonation (Carvalho et al., 2021; Casanova et al., 2021). It was claimed that the precipitation of $CaCO_3$ and sodium carbonates was responsible for the strength increase. One possible explanation is that the formation of these phases could promote the polymerization of the Si-O-Si and Si-O-Al gels (Casanova et al., 2021). However, more research is needed in this area.

5. AAM prepared with MSWI bottom ash and other industrial by-products as precursor

In previous studies, MSWI bottom ash was used together with other industrial by-products to prepare AAM (see Appendix Table 4). These industrial by-products include blast furnace slag (Huang et al., 2020b, 2020a, 2019a, 2018; Jin et al., 2021), metakaolin (Lancellotti et al., 2013; Zhu et al., 2018b), coal fly ash (Wongsa et al., 2017), waste glass (Xuan et al., 2019), and secondary aluminum recycling by-product (PAVAL®) (Maldonado-Alameda et al., 2021b). Compared with waste glass and PAVAL®, blast furnace slag, metakaolin, and coal fly ash are more commonly used AAM precursors (Provis, 2018; Provis and Van Deventer, 2013). Waste glass was used by Xuan et al. (2019) to increase the content of reactive SiO_2 in MSWI bottom ash-based AAM. The PAVAL® was used by Maldonado-Alameda et al. (2021b) to compensate for the Al_2O_3 deficiency in MSWI bottom ash-based AAM. Binary AAM systems, including MSWI bottom ash-BFS, MSWI bottom ash-metakaolin, and MSWI bottom ash-coal fly ash, are discussed in the following section.

5.1. MSWI bottom ash and blast furnace slag

Blast furnace slag was used to partially replace MSWI bottom ash to increase the compressive strength of alkali-activated MSWI bottom ash. Huang et al. (2019a) found that the content of active calcium in BFS was more than two times as much as that in MSWI bottom ash. Replacing MSWI bottom ash with BFS can increase the active CaO content in the precursor, which is beneficial to the strength development of AAM. However, the residual metallic Al in MSWI bottom ash always leads to a strength decrease. This risk can be eliminated by treating MSWI bottom ash in NaOH solution (Huang et al., 2020b, 2020a, 2019a, 2019b, 2018; Jin et al., 2021). The MSWI bottom ash slurry obtained after NaOH solution treatment can be used directly to prepare AAM. Huang et al. (2020a) used thermally treated MSWI bottom ash as precursor to prepare alkali-activated mortars. NaOH solution treatment was used to reduce the metallic Al content in thermally treated MSWI bottom ash. In the end, the alkali-activated MSWI bottom ash mortar exhibited no volume expansion and had a 28-day compressive strength of 13.6 MPa. After replacing 40 wt.% MSWI bottom ash with BFS, the compressive strength of alkali-activated mortar increased by around 200 %.

The compressive strength of AAM prepared with blends of MSWI bottom ash and BFS not only depends on the metallic Al content of MSWI bottom ash and the mass ratios between MSWI bottom ash and BFS, but also on the type of activator and the curing conditions. Sealed curing at room temperature is found to be the optimal curing condition for the alkali-activated mortar prepared with MSWI bottom ash and BFS (Huang et al., 2018). Compared with NaOH solution and water glass solution, a mixture of NaOH solution and water glass solution is more suitable for activating blends of MSWI bottom ash and BFS. More C-S-H and C-A-S-H gels are formed when the mixture of NaOH solution and Na_2SiO_3 solution is used as activator, resulting in a higher compressive

strength (Huang et al., 2019a; Jin et al., 2021). Besides, the compressive strength of alkali-activated mortar prepared with blends of MSWI bottom ash and BFS can be optimized by modifying the molar ratio between SiO_2 and Na_2O in the mixture of NaOH solution and Na_2SiO_3 solution. For the alkali-activate mortar prepared with 60 wt.% MSWI bottom ash and 40 wt.% BFS, the highest compressive strength can be obtained at the SiO_2 to Na_2O molar ratio of 1.04 (Huang et al., 2019a).

MSWI bottom ash was also used as a mineral additive to enhance the properties of alkali-activated slag. Zhang et al. (2023) replaced 0–12 wt.% blast furnace slag with MSWI bottom ash to improve the high-temperature resistance of alkali-activated slag. The presence of metallic Al in MSWI bottom ash was observed to enhance the thermal resistance of AAM. This enhancement can be attributed to the generation of hydrogen gas after the reaction between metallic Al and activator. The entrainment of hydrogen gas in fresh alkali-activated paste improves its pore connectivity and contributes to a reduction in water vapor pressure and shrinkage, thus inhibiting matrix cracking in hardened alkali-activated paste. The optimal replacement level of MSWI bottom ash in alkali-activated slag was found to be 6 wt.% (Zhang et al., 2023).

5.2. MSWI bottom ash and coal fly ash

Wongsa et al. (2017) used MSWI bottom ash to replace Class F coal fly ash for the preparation of alkali-activated mortar. This MSWI bottom ash was derived from the combustion of dry branches, paper, and dry leaves collected at a Thai university. The compressive strength of alkali-activated mortar decreased as the percentages of MSWI bottom ash increased from 20 to 40 wt.% in the precursor. The 28-day compressive strength of alkali-activated mortar increased by 26 % when 20 wt.% Class F coal fly ash was replaced by MSWI bottom ash. At a replacement level of 40 wt.%, the compressive strength of alkali-activated MSWI bottom ash-Class F coal fly ash mortar was still slightly higher than the alkali-activated coal fly ash mortar. The higher compressive strength of alkali-activated MSWI bottom ash-Class F coal fly ash mortar was attributed to the small particle size and high CaO content of MSWI bottom ash. The average particle size of MSWI bottom ash was 5.15 μm, much smaller than that of Class F coal fly ash (32.58 μm). MSWI bottom ash contained 38.1 wt.% CaO, more than two times the CaO content in Class F coal fly ash (14.5 wt.%). Blending MSWI bottom ash with Class F coal fly ash increased the CaO content in the precursor, promoting the formation of C-S-H gel (Wongsa et al., 2017).

5.3. MSWI bottom ash and metakaolin

Lancellotti et al. (2013) studied the possibility of using MSWI bottom ash as an alternative to metakaolin for the preparation of alkali-activated paste. The maximum replacement level of MSWI bottom ash was 70 wt.%. The sample failed upon demolding when more than 70 wt.% metakaolin was replaced by MSWI bottom ash. According to analysis by SEM combined with Energy-Dispersive X-ray Spectroscopy (EDS), the mass ratio of Si/Al in the gel phases formed in alkali-activated MSWI bottom ash-metakaolin paste increased from 2.5 to 3.36 when the replacement level of MSWI bottom ash increased from 50 wt.% to 70 wt.%. This test result indicated that the Si ions dissolved from MSWI bottom ash could participate in the formation of gel phases (Lancellotti et al., 2013).

Zhu et al. (2018b) used the metallic Al-containing MSWI bottom ash as a gas-foaming agent to prepare aerated alkali-activated metakaolin paste. MSWI bottom ash was regarded as an alternative to Al powder rather than a replacement for metakaolin. The aeration capacity of MSWI bottom ash was about 1/250 that of Al powder. The rheological properties of alkali-activated metakaolin were almost independent of the incorporation of Al powder. In comparison, the addition of MSWI bottom ash delayed the setting and remarkably increased the yield stress and viscosity of the fresh paste. The porous alkali-activated metakaolin paste with MSWI bottom ash as a foaming agent showed similar compressive strength and thermal conductivity to that prepared with metallic Al.

6. Environmental impacts of MSWI bottom ash-based AAM

Previous life cycle impact assessment (LCIA) results have indicated that using MSWI bottom ash to prepare AAM is environmentally beneficial (Torelli, 2020). There are, however, very few studies in this area and life cycle assessment (LCA) is usually performed using the cradle-to-gate method according to ISO 14040 (2006) ("NEN Connect - ISO 14040," 2006).

Torelli (2020) assessed the environmental impacts of alkali-activated mortars with their precursor consisting of a blend of 40 wt.% MSWI bottom ash and 60 wt.% Class F coal fly ash (Wongsa et al., 2017) or a mixture of 60 wt.% MSWI bottom ash and 40 wt.% BFS (Huang et al., 2019a, 2018). The mix designs of the alkali-activated mortars were proposed by Wongsa et al. (2017) and Huang et al. (2019a, 2018), respectively. For life cycle assessment, the MSWI bottom ash used by Wongsa et al. (2017) and Huang et al. (2019a, 2018) were assumed to be the same. The life cycle inventory (LCI) data of MSWI bottom ash was obtained by assessing the environmental impacts of the plant-scale treatments required to transform freshly quenched MSWI bottom ash into fine powders suitable for being used as AAM precursor. The data about the plant-scale treatments was directly taken from the literature. The LCIA results showed that MSWI bottom ash blended alkali-activated mortars had a significantly lower impact on global warming than Portland cement mortar with the same compressive strength. However, the alkali-activated mortars had higher environmental footprints in other impact categories, including abiotic depletion, ozone layer depletion, photochemical oxidation, acidification, and eutrophication. Among all the constituents of alkali-activated mortars, Class F coal fly ash and BFS were the main contributors to these environmental impact categories (Torelli, 2020).

7. Conclusions

The use of municipal solid waste incineration (MSWI) bottom ash as precursor for alkali-activated materials (AAM) provides a sustainable solution for the recycling of this industrial by-product and contributes to the low-carbon transformation of construction materials. This review gives a comprehensive overview of current advances in using MSWI bottom ash to produce AAM. The conclusions of this review are summarized below:

- Although the compositions of MSWI bottom ash previously used to produce AAM vary significantly, certain elements and minerals are frequently detected in this ash. A thorough understanding of the frequently occurring constituents in MSWI bottom ash can pave the way for expanding its application as AAM precursor. Studying the chemical composition of the amorphous phase in MSWI bottom ash is crucial. This compositional information can help assess the reactivity of the MSWI bottom ash as AAM precursor and allows for predicting reaction products through thermodynamic modeling. The modeling result can serve as a reference to guide the mix design of alkali-activated MSWI bottom ash.
- Prior to the application as AAM precursor, MSWI bottom ash usually needs to be treated to improve its quality. While various methods have been proposed for this purpose, a standardized approach to evaluate their effectiveness is lacking. Most of these techniques have proven effective only at the laboratory scale. The challenge lies in cost-effectively upscaling these methods to an industrial level. Moreover, the quality requirements of treated MSWI bottom ash for the application as AAM precursor have not been clearly defined in existing studies.

- When using MSWI bottom ash to prepare AAM, the mix design is usually proposed based on a trial-and-error method. The most commonly used activator is a mixture of NaOH solution and water glass solution. The reaction mechanism and reaction products of MSWI bottom ash upon alkali activation have been extensively studied in previous research. The engineering performance of AAM derived from MSWI bottom ash is determined by its microstructure characteristics. However, the microstructure formation of alkali-activated MSWI bottom ash is rarely studied.
- The AAM prepared with 100 % MSWI bottom ash usually has very low compressive strength. Factors influencing the mechanical properties of alkali-activated MSWI bottom ash are the metallic Al content and reactivity of MSWI bottom ash, the type of activator, and the curing condition. In addition to these factors, the fresh properties of alkali-activated MSWI bottom ash are also influenced by the particle shape and water absorption of MSWI bottom ash.
- In most cases, the leaching of heavy metals from alkali-activated MSWI bottom ash is more severe than from unreacted MSWI bottom ash. Leaching of some heavy metals from alkali-activated MSWI bottom ash can exceed the regulatory upper limit. In previous research, MSWI bottom ash was blended with other types of precursors, such as blast furnace slag, metakaolin, and coal fly ash, to enhance the properties of AAM derived from MSWI bottom ash.
- Previous studies indicated that AAM prepared with MSWI bottom ash had lower environmental impacts than Portland cement-based construction materials. It is worth noting that there is very limited number of studies available regarding the environmental impacts of MSWI bottom ash-based AAM.
- At the moment, most of the research efforts are focused on exploring the potential and feasibility of utilizing MSWI bottom ash as precursor for the production of AAM. Current studies mainly reported the compressive strength of MSWI bottom ash-based AAM. There is a notable research gap when it comes to the durability and other mechanical properties of MSWI bottom ash-based AAM. Additionally, there is also a lack of information regarding the specific applications where the developed MSWI bottom ash-based AAM can be used. Addressing these gaps is crucial for promoting practical application and broader adoption of AAM made from MSWI bottom ash.

8. Recommendations

Although a lot of experience and knowledge has been accumulated regarding the development of MSWI bottom ash-based AAM, there is still a lot of work to be done before this construction material is accepted by the construction industry.

- Research about the reactivity and reaction mechanism of each constituent of MSWI bottom ash is required. After breaking the problem down to the study of individual reactive phase, the fundamental study of the interaction among these phases is possible. An in-depth understanding of the reactive phases in MSWI bottom ash can help to guide quality upgrade treatments of MSWI bottom ash.
- It is recommended to identify the correlation between the physico-chemical properties of the reaction products of MSWI bottom ash and the engineering properties of MSWI bottom ash-based AAM. Establishing this relationship is essential for optimizing and enhancing the properties of the AAM derived from MSWI bottom ash.
- The study about the fresh properties, long-term performance, durability, and leaching potential of MSWI bottom ash-based AAM is insufficient. However, this information is critical for the formulation of design codes when MSWI bottom ash is used as an ingredient of concrete. Once the legal guidelines are established, the widespread industrial application of MSWI bottom ash as a mineral resource for construction materials will be possible.
- The environmental impacts of AAM prepared with MSWI bottom ash are strongly influenced by the quality-upgrade treatments of MSWI bottom ash and the mix design. There is always a need to assess the environmental impacts of proposed quality-upgrade treatments and produced AAM to check whether these products are environmentally friendly.
- It is not recommended to use MSWI bottom ash as a sole precursor for AAM production due to concerns related to excessive heavy metal leaching and low mechanical strength. The future research should focus on developing blended AAM system. It is promising to use MSWI bottom ash in combination of other more reactive industrial-by products to eliminate the leaching risks of MSWI bottom ash and improve the mechanical properties of MSWI bottom ash-based AAM.
- It is important to keep track of the leaching of heavy metals over the life cycle of constructions containing MSWI bottom ash. Concrete elements that contain MSWI bottom ash should be registered. In this case, at the stage of demolition, it is possible to distinguish and separate the concretes made from MSWI bottom ash.

CRediT authorship contribution statement

Boyu Chen: Conceptualization, Data curation, Formal analysis, Visualization, Writing – original draft, Writing – review & editing. **Priyadharshini Perumal:** Data curation, Writing – original draft, Writing – review & editing. **Farnaz Aghabeyk:** Data curation, Writing – original draft, Writing – review & editing. **Adeolu Adediran:** Writing – original draft, Writing – review & editing. **Mirja Illikainen:** Supervision, Writing – review & editing. **Guang Ye:** Conceptualization, Supervision, Writing – review & editing.

Declaration of competing interest

The authors declare that they have no known competing financial interests or personal relationships that could have appeared to influence the work reported in this paper.

Data availability

The authors do not have permission to share data.

Acknowledgments

Boyu Chen would like to acknowledge financial support from the Chinese Scholarship Council (Grant No. 201708360087) and Mineralz (Part of Renewi). Priyadharshini Perumal wishes to acknowledge the financial support received from the SUSRES project funded by Academy of Finland-Academy Project (No. 347678) and the European Union's Horizon 2020 research and innovation program under the Marie Sklodowska Curie grant agreement No. 839848. Special acknowledgement is given to professor Klaas van Breugel for his help with the improvement of text writing.

Appendixes

Appendix Table 1
Chemical composition of MSWI bottom ash in different studies based on the origin.

Compound (wt.%)	China				Singapore			Spain				Italy	Thailand	Portugal	UK	The Netherlands		Oxide Range (wt.%)
	(Huang et al., 2020b, 2019a, 2018; Jin et al., 2021)	(Xuan et al., 2019)	(Huang et al., 2020a)	(Zhang et al., 2023)	(Chen et al., 2016)	(Zhu et al., 2018a, 2018b)	(Zhu et al., 2019c)	(Maldonado-Alameda et al., 2020a)	(Maldonado-Alameda et al., 2020b, 2021b)	(Maldonado-Alameda et al., 2023)		(Lancellotti et al., 2015)	(Wongsa et al., 2017)	(Carvalho et al., 2021; Casanova et al., 2021)	(Qiao et al., 2008c, 2008b)	(Chen et al., 2020)	(Chen et al., 2023b)	
SiO_2	58.82	37.72	51.82	21.68	32.75	29.70	43.90	45.44	52.08	37.2	64.5	45–48	15.80	51.84	36.20	38.79	52.91	15.80–64.5
Al_2O_3	14.18	8.46	14.18	5.76	8.57	7.77	6.55	10.38	6.35	9.30	4.97	9–10	0.90	5.00	8.48	7.15	10.18	0.9–14.18
CaO	14.44	21.60	16.44	54.21	29.06	26.35	25.89	17.55	20.72	24.6	14.7	17–19	38.10	23.00	20.20	10.75	13.44	10.75–54.21
Fe_2O_3	6.18	3.95	6.18	6.29	10.02	9.09	10.13	6.08	4.12	8.50	4.31	4–5	4.20	9.29	6.21	28.77	9.29	3.95–28.77
Na_2O	2.24	2.52	2.24	–	2.87	2.60	4.61	5.04	3.38	1.10	1.03	6–8*	0.20	–	2.93	3.27	4.24	1.57–8*
K_2O	2.52	1.61	2.52	1.77	1.24	1.12	1.08	1.54	2.09	1.80	2.45		7.30	1.57	1.04	0.51	0.84	
MgO	3.26	1.75	3.26	2.10	1.75	1.58	1.76	2.66	2.43	1.70	1.17	2–3	3.50	2.36	1.58	1.79	2.40	1.58–3.5
SO_3	–	2.33	–	–	3.01	2.73	–	2.57	1.07	1.74	1.07	–	1.50	2.42	2.34	0.60	0.70	0.60–3.01
P_2O_5	–	4.02	–	–	4.77	4.33	3.96	–	–	1.55	1.60	–	1.70	2.29	1.59	–	1.03	1.59–4.77
ZnO	–	–	–	–	0.81	0.73	0.36	–	–	–	–	–	–	–	0.37	0.47	0.55	0.36–0.81
PbO	–	–	–	–	0.12	0.11	0.13	–	–	–	–	–	–	–	0.24	0.09	0.09	0.09–0.24
CuO	–	–	–	–	0.31	0.28	0.21	–	–	–	–	–	–	0.16	0.30		0.31	0.16–0.31
LOI	1.62	12.64	1.62	–	–	9.30	Assumed insignificant	5.78	6.10	8.75	2.40	7–10	23	–	12.80		2.17	–

*Sum of alkali oxides (K_2O and Na_2O).

Appendix Table 2
Mineralogical composition of MSWI bottom ash in different studies based on the origin.

Origin of bottom ash	Categories																		References
	Silicon dioxide (Quartz)	Carbonates		Silicates									Iron oxides			Non-ferrous metal oxides		Other minerals	
				Sorosilicates		Tectosilicates			Inosilicates			Other Silicates							
		Calcite	Dolomite	Gehlenite	Akermanite	Albite	Anorthite	Microcline	Ortho pyroxene	Diopside	(Pseudo) Wollastonite		Magnetite	Wustite	Hematite	Rutile	Corundom		
China	✓	✓	–	–	–	–	–	–	–	–	–	–	–	–	–	–	✓	Metallic aluminum	(Huang et al., 2019a)
	✓	✓	–	–	–	–	–	–	–	–	–	–	–	–	–	–	✓	Calcium-sodium-magnesium phosphate	(Xuan et al., 2019)
Italy	✓	✓	–	✓	–		–	–	–	–	–	Ca, Na Silicate ($Na_8Ca_3Si_5O_{17}$)	–	–	–	–	–	–	(Lancellotti et al., 2015)
Portugal	✓	✓	–	–	–	–	✓	–	–	–	–	–	✓	–	–	✓	–	kamacite	(Carvalho et al., 2021; Casanova et al., 2021)
Singapore	✓	✓	–	–	–	–	–	–	–	–	–	–	✓	–	–	–	–	Hydroxyl apatite	(Zhu et al., 2018a)
	✓	✓	–	–	–	–	–	–	–	–	–	–	✓	–	–	–	–	–	(Chen et al., 2016)
Spain	✓	✓	–	–	✓	–	–	✓	–	–	✓	Muscovite, Kyanite,	✓	–	–	–	–	Hydrocalumite	(Maldonado-Alameda et al., 2020a)
	✓	✓	✓	–	✓	✓	–	✓	–	–	–	Muscovite	–	–	–	–	–	Anhydrite	(Maldonado-Alameda et al., 2020b, 2021b)
	✓	✓	–	–	✓	–	✓	✓	–	–	–	–	✓	–	–	–	–	Hydrocalumite	(Maldonado-Alameda et al., 2023)
	✓	✓	–	–	–	–	✓	✓	–	–	✓	–	–	–	✓	–	–	–	
Thailand	✓	✓	–	–	–		–	–	–	–	–	–	–	–	–	–	–	–	(Wongsa et al., 2017)
UK	✓	✓	–	–	–		–	–	–	–		–	✓			–	–	–	(Qiao et al., 2008c, 2008b)
The Netherlands	✓	✓	–	✓	–	✓	–	–	–	✓	✓	–	✓	✓	✓	–	✓	Goethite	(Chen et al., 2020)
The Netherlands	✓	✓	–	✓	–	✓	–	–	✓	✓	✓	–	✓	✓	✓	–	✓	Halite, Phosphammite, Goethite, Iron, Gibbsite	(Chen et al., 2023b)

Appendix Table 3
Summary of studies reporting utilization of MSWI bottom ash as precursor for alkali-activated materials.

Origin	AAM prepared using MSWI bottom ash as precursor												
	Information of used MSWI bottom ash and plant-scale treatments	Lab-scale treatments and metallic Al content (wt.%)	SiO_2 (wt.% from XRF)	Al_2O_3 (wt.% from XRF)	CaO (wt.% from XRF)	Binder: MSWI bottom ash (%)	Activators		Mix ratio	Curing conditions	Measured specimen size (mm)	Compressive strength (MPa) and Curing age (days)	References
China	Metallic Al content: 1.92 wt.%	Water washed + ball milled + NaOH solution treated (3 h) or calcinated (1050°C)	51.82	14.18	16.44	100	Na_2SiO_3 solution + NaOH solution	0.6 (liquid to binder ratio)	1:3 (M)	20 ± 2°C, 95 % RH	40 × 40 × 160	Original: 0^{3d} 2.4^{28d} After NaOH treatment: 1.9^{3d} 8.4^{28d} 10.3^{60d} After calcination: 3.8^{3d} 10.4^{28d} 13.3^{60d}	(Huang et al., 2020a)
Portugal	D_{50} = 45 μm Contains metallic Al (percentage unknown)	Ball milled Metallic Al: 0.44 (defoamed before casting)	51.84	5.00	23.00	100	Na_2SiO_3 solution or NaOH solution	0.65 (liquid to binder ratio) (2 % water reducer)	1:3 (M)	70°C (1d) then 20 ± 3°C, 50 % RH	40 × 40 × 160	90d NaOH activated samples: 6 - 7 90d Na_2SiO_3 activated samples: 1 - 4	(Carvalho et al., 2021)
Portugal	D_{50} = 45 μm Contains metallic Al (percentage unknown)	Ball milled Metallic Al: 0.44 (15 min mixing time + 45 min defoamed before casting)	51.84	5.00	23.00	100	NaOH solution (10M)	0.65 (water reducer)	1:3 (M)	18°C, 65 % RH (1d) or 70°C (1d) or 70°C (2d) or 90°C (1d) then 20°C, 60 % RH	40 × 40 × 160	112d: 15 - 30 90d flexural strength: 2 - 4	(Casanova et al., 2021)
Singapore	D_{50} < 20 μm (Fresh) Contains metallic Al (percentage unknown)	105°C 24 h	32.75	8.57	29.06	100	NaOH solution+ Na_2SiO_3 solution	0.6 or 0.75 or 0.9 (liquid to solid ratio)	P	75°C (3d)	50 × 50 × 50	3d: 0.95 - 2.82	(Chen et al., 2016)
Singapore	< 75 μm (Fresh)	Ball milled + sieved (only use the glass fraction)	67.64	1.76	9.81	100	NaOH solution (14 M) + Na_2SiO_3 solution Mass ratio: 1:2	0.5 (liquid to solid ratio)	P	75°C, 98 % RH – 3d	50 × 50 × 50	30.0^{3d}	(Zhu et al., 2019b)
Singapore	Glass fraction: < 75 μm, D_{50} = 16.9 μm Non-ferrous fraction: < 150 μm, D_{50} = 22.7 μm (> 1.18 mm fraction)	Manual separation + magnet separation + ball milled	68.04-69.05 Glass fraction: 30.5-40.2 Non-ferrous fraction	1.71-1.96 Glass fraction 8.87-10 Non-ferrous fraction	9.59-10.42 Glass fraction 24.16-30.1 Non-ferrous fraction	Glass fraction + non-ferrous fraction	NaOH solution (8 M) + Na_2SiO_3 solution SiO_2/Na_2O ratio = 1.57)	0.5 (solution to solid)	P	75°C 3d, 98 % RH	50 × 50 × 50	3d: 4.0 - 31.7	(Zhu et al., 2019c)

(*continued on next page*)

Appendix Table 3 (*continued*)

Origin	AAM prepared using MSWI bottom ash as precursor											
	Information of used MSWI bottom ash and plant-scale treatments	Lab-scale treatments and metallic Al content (wt.%)	SiO_2	Al_2O_3	CaO	Binder	Activators	Mix ratio	Curing conditions	Measured specimen size (mm)	Compressive strength (MPa) and Curing age (days)	References
			wt.% from XRF			MSWI bottom ash (%)						
	Fresh, original < 1 dm Contains metallic Al (percentage unknown)											
Spain	< 80 μm (Weathered 3 months) Contains metallic Al (percentage unknown)	Sieved + crushed (Jaw) + milled (disc mill)	45.44	10.38	17.55	100	Na_2SiO_3 solution+ NaOH solution Mass ratio 4:1	1 (liquid to solid ratio)	P	25 ± 1°C 95 ± 5 % RH (demold after 3 days)	25 × 25 × 25	28d: 4 - 7	(Maldonado-Alameda et al., 2020)
Spain	< 80 μm (As-received: 8 - 30 mm) Weathered (2 - 3 months) Contains metallic Al (percentage unknown)	Crushed + milled Contains metallic Al (percentage unknown)	52.08	6.35	20.72	100	Na_2SiO_3 solution+ NaOH solution Mass ratio: 4:1	0.8 (liquid to solid mass ratio)	P	25 ± 1°C > 95 ± 5 % RH	25 × 25 × 25 Demoulded after 3 days	28d(max.): 22.8	(Maldonado-Alameda et al., 2021a)
Spain	< 80 μm (Metal separation)	Drying + magnetic separation+crushing + milling)	37.2 64.5	9.3 4.97	24.6 14.7	100	NaOH solution+ Na_2SiO_3 solution (mass ratio 4:1)	Not mentioned	P	Room temperature or 70°C for 3 days, then demold and cure at room temperature and ambient relative humidity for 28-days	25 × 25 × 25 Demoulded after 3 days	28d: 5-8 28d: 7-11	(Maldonado-Alameda et al., 2023)
UK	< 200 μm (weathered, as received < 14 mm) Contains metallic Al (percentage unknown)	Milled (hammer + ball) + thermally treated (800°C)	36.2	8.48	20.20	90	Hydrated lime (10 wt.% of dry mix)	0.5 0.2 (water to solid ratio)	P	Condition 1: 20°C, 98 % RH (3d), then demold Condition 2: 20°C, 98 % RH (7d) + lime water immersion (21d)	20 (diameter) × 40	7d: 0.5 - 12.7 28d: 1.1 - 14.7	(Qiao et al., 2008c)
UK	< 200 μm (weathered, original < 14 mm) Contains metallic Al (percentage unknown)	Hammer milled + ball milled + thermally treated (600, 700, 800, 880°C)	36.2	8.48	29.20	100	Hydrated lime	0.5 (water to solid ratio)	P	Demold after 3 days	20 (diameter) × 40	28d: 0.5 - 3	(Qiao et al., 2008b)

D50: Mean particle size, RH: Relative humidity, M: Mortar, P: Paste, d: day

Appendix Table 4
Summary of studies reporting utilization of MSWI bottom ash and other industrial by-products as precursors for alkali-activated materials.

Origin	AAM prepared using MSWI bottom ash and other industrial by-products as precursor													
	Information of used MSWI bottom ash and plant-scale treatments	Lab-scale treatment and metallic Al content (wt. %)	SiO_2 (wt.% from XRF)	Al_2O_3 (wt.% from XRF)	CaO (wt.% from XRF)	Binder: MSWI bottom ash (%)	Binder: Others (%)	Activators		Mix ratio	Curing condition	Analyzed specimen size (mm)	Compressive strength (MPa) and Curing age (days)	References
China	D_{50} = 47 μm Contains metallic Al (percentage unknown)	Ground + sieved + NaOH defoamed	53.82	14.18	14.44	60	BFS	NaOH + Na_2SiO_3	0.6 (liquid to binder ratio)	1:3 (M)	Sealed, 20 ± 2 °C, > 95 % RH	40 × 40 × 160	53.7^{28d} 56.3^{60d}	(Huang et al., 2018)
China	Contains metallic Al (percentage unknown)	Ball milled Alkali-treated	53.82	14.18	14.44	60	BFS	NaOH + Na_2SiO_3 (NaOH pellets percentage in the activator: 0 - 16.9 wt.%)	0.5	1:3 (M)	20 ± 2 °C, > 95 % RH	40 × 40 × 160	28d: 4.7 - 47.4 60d: 5.2 - 50.6	(Huang et al., 2020b)
China	D_{50} = 47 μm Contains metallic Al (percentage unknown)	Sieving + NaOH defoaming	53.8	14.2	14.4	60	BFS	NaOH + Na_2SiO_3 (SiO_2/Na_2O molar ratio: 0 - 1.14)	0.5 (liquid to binder ratio)	1:3 (M)	20 ± 2 °C, > 95 % RH	40 × 40 × 160	Max: 49.6^{28d}, 53.4^{60d}	(Huang et al., 2019a)
China	Metallic Al content: 1.92 wt.%	Water washed + ball milled + calcinated (700 °C) + NaOH treatment(3 h)	51.82	14.18	16.44	60	BFS	Na_2SiO_3 + NaOH	0.6 (liquid to binder ratio)	1:3 (M)	20 ± 2 °C, 95 % RH	40 × 40 × 160	40.6^{28d} 45.4^{60d}	(Huang et al., 2020a)
China	D_{50} = 18.44 μm (original: < 2.36 mm)	Sieved + oven dried + ball milled Metallic Al content: 0.048	37.72	8.46	21.6	0–80	Waste glass	NaOH	0.4 - 0.8 (liquid to solid ratio)	P	Steam curing, 80 °C	50 (diameter) × 100	28-day: 0.86 - 21	(Xuan et al., 2019)
China	D_{50} = 49 μm	Dried + ball milled	53.82	14.18	14.44	60	BFS	NaOH Or Na_2SiO_3 Or Na_2SiO_3 + NaOH	0.5 (liquid to solid ratio)	1:3 (M)	20 ± 2 °C, > 95 % RH	40 × 40 × 160	NaOH activated: 28d:0.8 - 25.7 60d:1.2 - 29.4 Na_2SiO_3 activated: 3d: 5.6 - 8.4 28d: 7.5 - 12.2 60d: 8.2 - 14.4 Na_2SiO_3 + NaOH activated: 28d: 34.7 - 43.1 60d: 38.6 - 48.2	(Jin et al., 2021)
China	D_{50} = 10 μm Metallic Al content (0.001 wt.%)	No treatment	21.68	5.76	54.21	0–12	BFS	Na_2SiO_3 + NaOH (Na_2O equivalent: 4 %, modulus 1.5)	0.35 (water to binder ratio)	P	25 ± 2 °C (1st day) 25 ± 1 C, 95 % RH (after the 1st day)	40 × 40 × 160	28d: 50 - 65	(Zhang et al., 2023)
Singapore	< 150 μm Contains metallic Al (percentage unknown)	Oven dried + ball milled	29.7	7.77	26.35	7.5–17.5	Metakaolin	Na_2SiO_3 + NaOH	1.36 (activator to metakaolin mass ratio)	P	28 ± 3 °C 84 ± 10 % RH	50 × 50 × 50	3d: 5.5 - 10.9	(Zhu et al., 2018b)

(*continued on next page*)

Appendix Table 4 (*continued*)

Origin	AAM prepared using MSWI bottom ash and other industrial by-products as precursor												
	Information of used MSWI bottom ash and plant-scale treatments	Lab-scale treatment and metallic Al content (wt. %)	SiO_2	Al_2O_3	CaO	Binder		Activators		Mix ratio	Curing condition	Analyzed specimen size (mm)	Compressive strength (MPa) and Curing age (days)	References
			wt.% from XRF			MSWI bottom ash (%)	Others (%)							
Spain	< 80 μm (weathered, 8–30 mm)	Crushed + milled	52.08	6.35	20.72	90–98	PAVAL® (secondary aluminum recycling by-product)	Na_2SiO_3 + NaOH (Na_2O respect to the total solid: 5.2 %, 5.8 %; SiO_2/Na_2O molar ratio: 2.3, 2.5)	0.6	P	25 ± 1 C, 95 ± 5 % RH (demold after 3 days)	25 × 25 × 25	28d: 11 - 26	(Maldonado-Alameda et al., 2021b)
Thailand	< 45 μm D_{50} = 5.15 μm	Ball milled	15.8	0.9	38.1	0–40	Coal Fly ash	NaOH (10 M) + Na_2SiO_3 (mass ratio: 1:1)	0.65 (liquid to binder ratio)	1:2.75 (M)	60 °C for 2days, then in controlled room at 25 °C, 50 % RH	50 × 50 × 50	9.2^{7d} 10.6^{28d}	(Wongsa et al., 2017)

D50: Mean particle size, RH: Relative humidity, M: Mortar, P: Paste, d: day.

References

Alam, Q., Schollbach, K., Rijnders, M., van Hoek, C., van der Laan, S., Brouwers, H.J.H., 2019. The immobilization of potentially toxic elements due to incineration and weathering of bottom ash fines. J. Hazard. Mater. 379 https://doi.org/10.1016/j.jhazmat.2019.120798.

Alnahhal, M.F., Kim, T., Hajimohammadi, A., 2021. Waste-derived activators for alkali-activated materials: a review. Cem. Concr. Compos. 118, 103980 https://doi.org/10.1016/j.cemconcomp.2021.103980.

Andrew, R.M., 2018. Global CO_2 emissions from cement production. Earth Syst. Sci. Data 10, 195–217.

Apostoli, P., Giusti, S., Bartoli, D., Perico, A., Bavazzano, P., Alessio, L., 1998. Multiple exposure to arsenic, antimony, and other elements in art glass manufacturing. Am. J. Ind. Med. 34, 65–72.

Arbi, K., Nedeljkovic, M., Zuo, Y., Ye, G., 2016. A review on the durability of alkali-activated fly ash/slag systems: advances, issues, and perspectives. Ind. Eng. Chem. Res. 55, 5439–5453.

Bernal, S.A., Provis, J.L., 2014. Durability of alkali-activated materials: progress and perspectives. J. Am. Ceram. Soc. 97, 997–1008.

Bernal, S.A., Provis, J.L., Brice, D.G., Kilcullen, A., Duxson, P., van Deventer, J.S.J., 2012. Accelerated carbonation testing of alkali-activated binders significantly underestimates service life: the role of pore solution chemistry. Cem. Concr. Res. 42, 1317–1326. https://doi.org/10.1016/j.cemconres.2012.07.002.

Bernal, S.A., Provis, J.L., Walkley, B., San Nicolas, R., Gehman, J.D., Brice, D.G., Kilcullen, A.R., Duxson, P., van Deventer, J.S.J., 2013. Gel nanostructure in alkali-activated binders based on slag and fly ash, and effects of accelerated carbonation. Cem. Concr. Res. 53, 127–144. https://doi.org/10.1016/j.cemconres.2013.06.007.

Blasenbauer, D., Huber, F., Lederer, J., Quina, M.J., Blanc-Biscarat, D., Bogush, A., Bontempi, E., Blondeau, J., Chimenos, J.M., Dahlbo, H., Fagerqvist, J., Giro-Paloma, J., Hjelmar, O., Hyks, J., Keaney, J., Lupsea-Toader, M., O'Caollai, C.J., Orupõld, K., Pająk, T., Simon, F.G., Svecova, L., Šyc, M., Ulvang, R., Vaajasaari, K., Caneghem, J.Van, van Zomeren, A., Vasarevičius, S., Wégner, K., Fellner, J., 2020. Legal situation and current practice of waste incineration bottom ash utilisation in Europe. Waste Manag. 102, 868–883. https://doi.org/10.1016/j.wasman.2019.11.031.

Boesch, M.E., Hellweg, S., 2010. Identifying improvement potentials in cement production with life cycle assessment. Environ. Sci. Technol. 44, 9143–9149.

Carvalho, R., Silva, R.V., de Brito, J., Pereira, M.F.C., 2021. Alkali activation of bottom ash from municipal solid waste incineration: optimization of NaOH- and Na 2SiO3-based activators. J. Clean. Prod. 291 https://doi.org/10.1016/j.jclepro.2021.125930.

Casanova, S., Silva, R.V., de Brito, J., Pereira, M.F.C., 2021. Mortars with alkali-activated municipal solid waste incinerator bottom ash and fine recycled aggregates. J. Clean. Prod. 289 https://doi.org/10.1016/j.jclepro.2020.125707.

Chancey, R.T., Stutzman, P., Juenger, M.C.G., Fowler, D.W., 2010. Comprehensive phase characterization of crystalline and amorphous phases of a Class F fly ash. Cem. Concr. Res. 40, 146–156. https://doi.org/10.1016/j.cemconres.2009.08.029.

Chen, B., Chen, J., de Mendonça Filho, F.F., Sun, Y., van Zijl, M.B., Copuroglu, O., Ye, G., 2024. Characterization and mechanical removal of metallic aluminum (Al) embedded in weathered municipal solid waste incineration (MSWI) bottom ash for application as supplementary cementitious material. Waste Manag. 176, 128–139. https://doi.org/10.1016/j.wasman.2024.01.031.

Chen, B., Perumal, P., Illikainen, M., Ye, G., 2023a. A review on the utilization of municipal solid waste incineration (MSWI) bottom ash as a mineral resource for construction materials. J. Build. Eng. 106386 https://doi.org/10.1016/j.jobe.2023.106386.

Chen, B., van Zijl, M.B., Keulen, A., Ye, G., 2020. Thermal treatment on MSWI bottom ash for the utilisation in alkali activated materials. KnE Eng. https://doi.org/10.18502/keg.v5i4.6792.

Chen, B., Zuo, Y., Zhang, S., de Lima Junior, L.M., Liang, X., Chen, Y., van Zijl, M.B., Ye, G., 2023b. Reactivity and leaching potential of municipal solid waste incineration (MSWI) bottom ash as supplementary cementitious material and precursor for alkali-activated materials. Constr. Build. Mater. 409, 133890 https://doi.org/10.1016/j.conbuildmat.2023.133890.

Chen, D., Zhang, Y., Xu, Y., Nie, Q., Yang, Z., Sheng, W., Qian, G., 2022. Municipal solid waste incineration residues recycled for typical construction materials—A review. RSC Adv 12, 6279–6291.

Chen, Z., Liu, Y., Zhu, W., Yang, E.H., 2016. Incinerator bottom ash (IBA) aerated geopolymer. Constr. Build. Mater. 112, 1025–1031. https://doi.org/10.1016/j.conbuildmat.2016.02.164.

Chimenos, J.M., Segarra, M., Fernandez, M.A., Espiell, F., 1999. Characterization of the bottom ash in municipal solid waste incinerator. J. Hazard. Mater. A.

Cong, P., Cheng, Y., 2021. Advances in geopolymer materials: a comprehensive review. J. Traffic Transp. Eng. (English Ed. 8, 283–314. https://doi.org/10.1016/j.jtte.2021.03.004.

Criado, M., Fernández-Jiménez, A., Palomo, A., Sobrados, I., Sanz, J., 2008. Effect of the SiO2/Na2O ratio on the alkali activation of fly ash. Part II: 29Si MAS-NMR Survey. Microporous Mesoporous Mater. 109, 525–534.

Damtoft, J.S., Lukasik, J., Herfort, D., Sorrentino, D., Gartner, E.M., 2008. Sustainable development and climate change initiatives. Cem. Concr. Res. 38, 115–127. https://doi.org/10.1016/j.cemconres.2007.09.008.

den Heede, P., De Belie, N., 2012. Environmental impact and life cycle assessment (LCA) of traditional and 'green' concretes: literature review and theoretical calculations. Cem. Concr. Compos. 34, 431–442.

Dou, X., Ren, F., Nguyen, M.Q., Ahamed, A., Yin, K., Chan, W.P., Chang, V.W.C., 2017. Review of MSWI bottom ash utilization from perspectives of collective characterization, treatment and existing application. Renew. Sustain. Energy Rev. https://doi.org/10.1016/j.rser.2017.05.044.

Duxson, P., Provis, J.L., Lukey, G.C., Mallicoat, S.W., Kriven, W.M., van Deventer, J.S.J., 2005. Understanding the relationship between geopolymer composition, microstructure and mechanical properties. Colloids Surfaces A Physicochem. Eng. Asp. 269, 47–58. https://doi.org/10.1016/j.colsurfa.2005.06.060.

Eurostat (Statistical Office of the European Communities), 2023. Municipal waste statistics [WWW Document]. URL https://ec.europa.eu/eurostat/statistics-explained/index.php?title=Municipal_waste_statistics#Municipal_waste_generation.

Fernández-Jiménez, A., Palomo, A., 2005. Mid-infrared spectroscopic studies of alkali-activated fly ash structure. Microporous mesoporous Mater. 86, 207–214.

García Lodeiro, I., Macphee, D.E., Palomo, A., Fernández-Jiménez, A., 2009. Effect of alkalis on fresh C–S–H gels. FTIR analysis. Cem. Concr. Res. 39, 147–153. https://doi.org/10.1016/j.cemconres.2009.01.003.

Giro-Paloma, J., Maldonado-Alameda, A., Formosa, J., Barbieri, L., Chimenos, J.M., Lancellotti, I., 2017. Geopolymers based on the valorization of Municipal Solid Waste Incineration residues. In: IOP Conference Series: Materials Science and Engineering. Institute of Physics Publishing. https://doi.org/10.1088/1757-899X/251/1/012125.

Grand View Research, 2019. Waste To Energy Market Size | Industry Report, 2020-2027 [WWW Document]. URL https://www.grandviewresearch.com/industry-analysis/waste-to-energy-technology-industry.

Habert, G., 2013. A method for allocation according to the economic behaviour in the EU-ETS for by-products used in cement industry. Int. J. Life Cycle Assess. 18, 113–126.

Habert, G., De Lacaillerie, J.B.D., Roussel, N., 2011. An environmental evaluation of geopolymer based concrete production: reviewing current research trends. J. Clean. Prod. 19, 1229–1238.

Habert, G., Ouellet-Plamondon, C., 2016. Recent update on the environmental impact of geopolymers. RILEM Tech. Lett. 1, 17–23.

Heath, A., Paine, K., McManus, M., 2014. Minimising the global warming potential of clay based geopolymers. J. Clean. Prod. 78, 75–83.

Huang, G., Ji, Y., Li, J., Zhang, L., Liu, X., Liu, B., 2019a. Effect of activated silica on polymerization mechanism and strength development of MSWI bottom ash alkali-activated mortars. Constr. Build. Mater. 201, 90–99. https://doi.org/10.1016/j.conbuildmat.2018.12.125.

Huang, G., Ji, Y., Zhang, L., Li, J., Hou, Z., 2018. The influence of curing methods on the strength of MSWI bottom ash-based alkali-activated mortars: the role of leaching of OH− and free alkali. Constr. Build. Mater. 186, 978–985. https://doi.org/10.1016/j.conbuildmat.2018.07.224.

Huang, G., Yang, K., Chen, L., Lu, Z., Sun, Y., Zhang, X., Feng, Y., Ji, Y., Xu, Z., 2020a. Use of pretreatment to prevent expansion and foaming in high-performance MSWI bottom ash alkali-activated mortars. Constr. Build. Mater. 245 https://doi.org/10.1016/j.conbuildmat.2020.118471.

Huang, G., Yang, K., Sun, Y., Lu, Z., Zhang, X., Zuo, L., Feng, Y., Qian, R., Qi, Y., Ji, Y., Xu, Z., 2020b. Influence of NaOH content on the alkali conversion mechanism in MSWI bottom ash alkali-activated mortars. Constr. Build. Mater. 248 https://doi.org/10.1016/j.conbuildmat.2020.118582.

Huang, G., Yuan, L., Ji, Y., Liu, B., Xu, Z., 2019b. Cooperative action and compatibility between Portland cement and MSWI bottom ash alkali-activated double gel system materials. Constr. Build. Mater. 209, 445–453. https://doi.org/10.1016/j.conbuildmat.2019.03.141.

International Energy Agency (IEA), 2009. Cement technology roadmap: carbon emissions reductions up to 2050 [WWW Document]. URL https://www.iea.org/reports/cement-technology-roadmap-carbon-emissions-reductions-up-to-2050.

International Renewable Energy Agency (IRENA), 2022. Renewable capacity statistics 2022 [WWW Document]. URL https://www.irena.org/-/media/Files/IRENA/Agency/Publication/2022/Apr/IRENA_RE_Capacity_Statistics_2022.pdf?rev=460f190dea15442eba8373d9625341ae.

Jin, L., Huang, G., Li, Y., Zhang, X., Ji, Y., Xu, Z., 2021. Positive influence of liquid sodium silicate on the setting time, polymerization, and strength development mechanism of mswi bottom ash alkali-activated mortars. Materials (Basel) 14. https://doi.org/10.3390/ma14081927.

Joseph, A.M., Matthys, S., De Belie, N., 2019. Reactivity of municipal solid waste incineration ashes as a supplementary cementitious material. In: 15th Int. Congress on the Chemistry of Cement (ICCC19). ICCC.

Kaza, S., Yao, L., Bhada-Tata, P., Van Woerden, F., 2018. What a Waste 2.0: a Global Snapshot of Solid Waste Management to 2050. The World Bank.

Kulik, D.A., Wagner, T., Dmytrieva, S.V., Kosakowski, G., Hingerl, F.F., Chudnenko, K.V., Berner, U.R., 2013. GEM-Selektor geochemical modeling package: revised algorithm and GEMS3K numerical kernel for coupled simulation codes. Comput. Geosci. 17, 1–24.

Kumar, V., Garg, N., 2022. The chemical and physical origin of incineration ash reactivity in cementitious systems. Resour. Conserv. Recycl. 177, 106009 https://doi.org/10.1016/j.resconrec.2021.106009.

Kurda, R., Silva, R.V., de Brito, J., 2020. Incorporation of alkali-activated municipal solid waste incinerator bottom ash in mortar and concrete: a critical review. Materials (Basel) 13, 3428.

Lancellotti, I., Cannio, M., Bollino, F., Catauro, M., Barbieri, L., Leonelli, C., 2015. Geopolymers: an option for the valorization of incinerator bottom ash derived "end of waste. Ceram. Int. 41, 2116–2123. https://doi.org/10.1016/j.ceramint.2014.10.008.

Lancellotti, I., Ponzoni, C., Barbieri, L., Leonelli, C., 2013. Alkali activation processes for incinerator residues management. Waste Manag. 33, 1740–1749. https://doi.org/10.1016/j.wasman.2013.04.013.

Li, M., Xiang, J., Hu, S., Sun, L., Su, S., Li, P., Sun, X., 2004. Characterization of solid residues from municipal solid waste incinerator. Fuel 83, 1397–1405.
Lin, K.L., Lin, D.F., 2006. Hydration characteristics of municipal solid waste incinerator bottom ash slag as a pozzolanic material for use in cement. Cem. Concr. Compos. 28, 817–823. https://doi.org/10.1016/j.cemconcomp.2006.03.003.
Liu, X., Li, S., Ding, Y., Lu, Z., Stephan, D., Chen, Y., Wang, Z., Cui, S., 2023. Investigation on admixtures applied to alkali-activated materials: a review. J. Build. Eng. 64, 105694 https://doi.org/10.1016/j.jobe.2022.105694.
Maldonado-Alameda, A., Giro-Paloma, J., Alfocea-Roig, A., Formosa, J., Chimenos, J.M., 2020a. Municipal solid waste incineration bottom ash as sole precursor in the alkali-activated binder formulation. Appl. Sci. 10 https://doi.org/10.3390/APP10124129.
Maldonado-Alameda, A., Giro-Paloma, J., Mañosa, J., Formosa, J., Chimenos, J.M., 2021a. Alkali-activated binders based on the coarse fraction of municipal solid waste incineration bottom ash. Boletín la Soc. Española Cerámica y Vidr. https://doi.org/10.1016/j.bsecv.2020.12.002.
Maldonado-Alameda, A., Giro-Paloma, J., Mañosa, J., Formosa, J., Chimenos, J.M., 2020b. Alkali-activated binders based on the coarse fraction of municipal solid waste incineration bottom ash. Bol. la Soc. Esp. Ceram. y Vidr. https://doi.org/10.1016/j.bsecv.2020.12.002.
Maldonado-Alameda, A., Giro-Paloma, J., Svobodova-Sedlackova, A., Formosa, J., Chimenos, J.M., 2020c. Municipal solid waste incineration bottom ash as alkali-activated cement precursor depending on particle size. J. Clean. Prod. 242 https://doi.org/10.1016/j.jclepro.2019.118443.
Maldonado-Alameda, A., Mañosa, J., Giro-Paloma, J., Formosa, J., Chimenos, J.M., 2021b. Alkali-activated binders using bottom ash from waste-to-energy plants and aluminium recycling waste. Appl. Sci. 11 https://doi.org/10.3390/app11093840.
Maldonado-Alameda, A., Mañosa, J., Miro-Escola, J., Quintero-Payan, A.C., Chimenos, J. M., 2023. Fluidised-bed incineration bottom ash as the sole precursor of alkali-activated binders: a comparison with bottom ash from grate incinerators. Constr. Build. Mater. 364 https://doi.org/10.1016/j.conbuildmat.2022.130001.
Manz, O.E., 1999. Coal fly ash: a retrospective and future look. Fuel 78, 133–136. https://doi.org/10.1016/S0016-2361(98)00148-3.
McLellan, B.C., Williams, R.P., Lay, J., Van Riessen, A., Corder, G.D., 2011. Costs and carbon emissions for geopolymer pastes in comparison to ordinary portland cement. J. Clean. Prod. 19, 1080–1090.
Mozgawa, W., Deja, J., 2009. Spectroscopic studies of alkaline activated slag geopolymers. J. Mol. Struct. 924, 434–441.
National Bureau of Statistics of China (NBS), 2022. Urban garbage collection and disposal situation [WWW Document]. URL https://data.stats.gov.cn/easyquery.htm?cn=E0103.
NEN Connect - ISO 14040, 2006.
Ng, T.S., Voo, Y.L., Foster, S.J., 2012. Sustainability With Ultra-High Performance and Geopolymer Concrete construction, in: Innovative Materials and Techniques in Concrete Construction. Springer, pp. 81–100.
Nodehi, M., Ozbakkaloglu, T., Gholampour, A., Mohammed, T., Shi, X., 2022. The effect of curing regimes on physico-mechanical, microstructural and durability properties of alkali-activated materials: a review. Constr. Build. Mater. 321, 126335 https://doi.org/10.1016/j.conbuildmat.2022.126335.
Pal, S.C., Mukherjee, A., Pathak, S.R., 2003. Investigation of hydraulic activity of ground granulated blast furnace slag in concrete. Cem. Concr. Res. 33, 1481–1486. https://doi.org/10.1016/S0008-8846(03)00062-0.
Pan, S.-Y., Du, M.A., Huang, I.-T., Liu, I.-H., Chang, E.-E., Chiang, P.-C., 2015. Strategies on implementation of waste-to-energy (WTE) supply chain for circular economy system: a review. J. Clean. Prod. 108, 409–421. https://doi.org/10.1016/j.jclepro.2015.06.124.
Phua, Z., Giannis, A., Dong, Z.L., Lisak, G., Ng, W.J., 2019. Characteristics of incineration ash for sustainable treatment and reutilization. Environ. Sci. Pollut. Res. 26, 16974–16997. https://doi.org/10.1007/s11356-019-05217-8.
Provis, J.L., 2018. Alkali-activated materials. Cem. Concr. Res. 114, 40–48. https://doi.org/10.1016/j.cemconres.2017.02.009.
Provis, J.L., Van Deventer, J.S.J., 2013. Alkali Activated materials: State-Of-The-Art report, RILEM TC 224-AAM. Springer Science \& Business Media.
Prud'homme, E., Autef, A., Essaidi, N., Michaud, P., Samet, B., Joussein, E., Rossignol, S., 2013. Defining existence domains in geopolymers through their physicochemical properties. Appl. Clay Sci. 73, 26–34. https://doi.org/10.1016/j.clay.2012.10.013.
Qiao, X.C., Ng, B.R., Tyrer, M., Poon, C.S., Cheeseman, C.R., 2008a. Production of lightweight concrete using incinerator bottom ash. Constr. Build. Mater. 22, 473–480. https://doi.org/10.1016/j.conbuildmat.2006.11.013.
Qiao, X.C., Tyrer, M., Poon, C.S., Cheeseman, C.R., 2008b. Characterization of alkali-activated thermally treated incinerator bottom ash. Waste Manag. 28, 1955–1962. https://doi.org/10.1016/j.wasman.2007.09.007.
Qiao, X.C., Tyrer, M., Poon, C.S., Cheeseman, C.R., 2008c. Novel cementitious materials produced from incinerator bottom ash. Resour. Conserv. Recycl. 52, 496–510. https://doi.org/10.1016/j.resconrec.2007.06.003.
Redden, R., Neithalath, N., 2014. Microstructure, strength, and moisture stability of alkali activated glass powder-based binders. Cem. Concr. Compos. 45, 46–56. https://doi.org/10.1016/j.cemconcomp.2013.09.011.
Rees, C.A., Provis, J.L., Lukey, G.C., van Deventer, J.S.J., 2007. Attenuated Total Reflectance Fourier Transform Infrared Analysis of Fly Ash Geopolymer Gel Aging. Langmuir 23, 8170–8179. https://doi.org/10.1021/la700713g.
Sabbas, T., Polettini, A., Pomi, R., Astrup, T., Hjelmar, O., Mostbauer, P., Cappai, G., Magel, G., Salhofer, S., Speiser, C., 2003. Management of municipal solid waste incineration residues. Waste Manag. 23, 61–88.
Silva, R.V., de Brito, J., Lynn, C.J., Dhir, R.K., 2017. Use of municipal solid waste incineration bottom ashes in alkali-activated materials, ceramics and granular applications: a review. Waste Manag. 68, 207–220. https://doi.org/10.1016/j.wasman.2017.06.043.
Sinton, C.W., LaCourse, W.C., 2001. Experimental survey of the chemical durability of commercial soda-lime-silicate glasses. Mater. Res. Bull. 36, 2471–2479.
Stengel, T., Heinz, D., Reger, J., 2009. Life cycle assessment of geopolymer concrete–what is the environmental benefit. In: Proceeding of the 24th Biennial Conference of the Concrete Institute of Australia.
Šyc, M., Simon, F.G., Hykš, J., Braga, R., Biganzoli, L., Costa, G., Funari, V., Grosso, M., 2020. Metal recovery from incineration bottom ash: state-of-the-art and recent developments. J. Hazard. Mater. 393, 122433 https://doi.org/10.1016/j.jhazmat.2020.122433.
Tang, P., Chen, W., Xuan, D., Zuo, Y., Poon, C.S., 2020. Investigation of cementitious properties of different constituents in municipal solid waste incineration bottom ash as supplementary cementitious materials. J. Clean. Prod. 258 https://doi.org/10.1016/j.jclepro.2020.120675.
Tang, P., Florea, M.V.A., Spiesz, P., Brouwers, H.J.H., 2016. Application of thermally activated municipal solid waste incineration (MSWI) bottom ash fines as binder substitute. Cem. Concr. Compos. 70, 194–205. https://doi.org/10.1016/j.cemconcomp.2016.03.015.
Tian, Y., Bourtsalas, A.C.(Thanos), Kawashima, S., Ma, S., Themelis, N.J., 2020. Performance of structural concrete using Waste-to-Energy (WTE) combined ash. Waste Manag. 118, 180–189. https://doi.org/10.1016/j.wasman.2020.08.016.
Torelli, D., 2020. Use of Waste Material in AAM concrete: Application in Circular Economy. Swiss Federal Institute of Technology Zurich.
United States Environmental Protection Agency (US EPA), 2022. National overview: facts and figures on materials, wastes and recycling [WWW Document]. URL https://www.epa.gov/facts-and-figures-about-materials-waste-and-recycling/national-overview-facts-and-figures-materials.
Verbinnen, B., Billen, P., Caneghem, J.Van, Vandecasteele, C., 2017. Recycling of MSWI bottom ash: a review of chemical barriers, engineering applications and treatment technologies. Waste Biomass Valoriz. 8, 1453–1466. https://doi.org/10.1007/s12649-016-9704-0.
Wagner, T., Kulik, D.A., Hingerl, F.F., Dmytrieva, S.V., 2012. GEM-Selektor geochemical modeling package: tSolMod library and data interface for multicomponent phase models. Can. Mineral. 50, 1173–1195.
Walkley, B., San Nicolas, R., Sani, M.-A., Rees, G.J., Hanna, J.V., van Deventer, J.S.J., Provis, J.L., 2016. Phase evolution of C-(N)-ASH/NASH gel blends investigated via alkali-activation of synthetic calcium aluminosilicate precursors. Cem. Concr. Res. 89, 120–135.
Wang, A., Zheng, Y., Zhang, Z., Liu, K., Li, Y., Shi, L., Sun, D., 2020. The durability of alkali-activated materials in comparison with ordinary Portland cements and concretes: a review. Engineering 6, 695–706. https://doi.org/10.1016/j.eng.2019.08.019.
Wang, W., Noguchi, T., 2020. Alkali-silica reaction (ASR) in the alkali-activated cement (AAC) system: a state-of-the-art review. Constr. Build. Mater. 252, 119105 https://doi.org/10.1016/j.conbuildmat.2020.119105.
Weil, M., Dombrowski, K., Buchwald, A., 2009. Life-cycle analysis of geopolymers. Geopolymers. Elsevier, pp. 194–210.
Wongsa, A., Boonserm, K., Waisurasingha, C., Sata, V., Chindaprasirt, P., 2017. Use of municipal solid waste incinerator (MSWI) bottom ash in high calcium fly ash geopolymer matrix. J. Clean. Prod. 148, 49–59. https://doi.org/10.1016/j.jclepro.2017.01.147.
Xia, Y., He, P., Shao, L., Zhang, H., 2017. Metal distribution characteristic of MSWI bottom ash in view of metal recovery. J. Environ. Sci. (China) 52, 178–189. https://doi.org/10.1016/j.jes.2016.04.016.
Xuan, D., Tang, P., Poon, C.S., 2019. MSWIBA-based cellular alkali-activated concrete incorporating waste glass powder. Cem. Concr. Compos. 95, 128–136. https://doi.org/10.1016/j.cemconcomp.2018.10.018.
Xuan, D., Tang, P., Poon, C.S., 2018. Limitations and quality upgrading techniques for utilization of MSW incineration bottom ash in engineering applications – A review. Constr. Build. Mater. 190, 1091–1102. https://doi.org/10.1016/j.conbuildmat.2018.09.174.
Xue, C., Sirivivatnanon, V., Nezhad, A., Zhao, Q., 2023. Comparisons of alkali-activated binder concrete (ABC) with OPC concrete - a review. Cem. Concr. Compos. 135, 104851 https://doi.org/10.1016/j.cemconcomp.2022.104851.
Yu, P., Kirkpatrick, R.J., Poe, B., McMillan, P.F., Cong, X., 1999. Structure of calcium silicate hydrate (C-S-H): near-, Mid-, and Far-infrared spectroscopy. J. Am. Ceram. Soc. 82, 742–748.
Zhang, B., Ma, Y., Yang, Y., Zheng, D., Wang, Y., Ji, T., 2023. Improving the high temperature resistance of alkali-activated slag paste using municipal solid waste incineration bottom ash. J. Build. Eng. 72 https://doi.org/10.1016/j.jobe.2023.106664.
Zhu, W., Chen, X., Struble, L.J., Yang, E.H., 2019a. Quantitative characterization of aluminosilicate gels in alkali-activated incineration bottom ash through sequential chemical extractions and deconvoluted nuclear magnetic resonance spectra. Cem. Concr. Compos. 99, 175–180. https://doi.org/10.1016/j.cemconcomp.2019.03.014.

Zhu, W., Chen, X., Struble, L.J., Yang, E.H., 2018a. Characterization of calcium-containing phases in alkali-activated municipal solid waste incineration bottom ash binder through chemical extraction and deconvoluted Fourier transform infrared spectra. J. Clean. Prod. 192, 782–789. https://doi.org/10.1016/j.jclepro.2018.05.049.

Zhu, W., Chen, X., Zhao, A., Struble, L.J., Yang, E.H., 2019b. Synthesis of high strength binders from alkali activation of glass materials from municipal solid waste incineration bottom ash. J. Clean. Prod. 212, 261–269. https://doi.org/10.1016/j.jclepro.2018.11.295.

Zhu, W., Rao, X.H., Liu, Y., Yang, E.H., 2018b. Lightweight aerated metakaolin-based geopolymer incorporating municipal solid waste incineration bottom ash as gas-forming agent. J. Clean. Prod. 177, 775–781. https://doi.org/10.1016/j.jclepro.2017.12.267.

Zhu, W., Teoh, P.J., Liu, Y., Chen, Z., Yang, E.H., 2019c. Strategic utilization of municipal solid waste incineration bottom ash for the synthesis of lightweight aerated alkali-activated materials. J. Clean. Prod. 235, 603–612. https://doi.org/10.1016/j.jclepro.2019.06.286.